Aryl hydrocarbon receptor activation promotes effector CD4$^+$ T cell homeostasis and restrains salt-sensitive hypertension

Patrick A. Molina*[1], Claudia J. Edell*[1], Luke S. Dunaway[1], Cailin E. Kellum[1], Rachel Q. Muir[2], Melissa S. Jennings[2], Jackson C. Colson[1], Carmen De Miguel[1], Megan K. Rhoads[1], Ashlyn A. Buzzelli[3], Laurie E. Harrington[3], Selene Meza-Perez[4], Troy D. Randall[4], Davide Botta[5,6], Dominik N. Müller[7,8,9], David M. Pollock[1], Craig L. Maynard[2], and Jennifer S. Pollock[1]‡

[1] Cardio-Renal Physiology and Medicine Section, Division of Nephrology, [2] Department of Pathology, [3] Department of Cell, Developmental and Integrative Biology, [4] Department of Medicine, Division of Clinical Immunology and Rheumatology, [5] Department of Microbiology, [6] Immunology Institute, Heersink School of Medicine, University of Alabama at Birmingham, Birmingham, AL USA 35223

[7] Experimental and Clinical Research Center, Max Delbrück Center for Molecular Medicine and Charité-Universitätsmedizin Berlin, [8] Max Delbrück Center for Molecular Medicine in the Helmholtz Association, Robert-Rössle-Str. 10, [9] Charité -Universitätsmedizin Berlin, Corporate Member of Freie Universität Berlin and Humboldt Universität Zu Berlin, Lindenberger Weg 80, Berlin 13092, Germany

*Equal contribution by these authors

‡Corresponding Author:
Jennifer S. Pollock, PhD
1918 University Blvd, MCLM515
CardioRenal Physiology and Medicine Section
Division of Nephrology, Department of Medicine
University of Alabama at Birmingham
Birmingham, AL 35223 USA
jenniferpollock@uabmc.edu

ABSTRACT

Excess dietary salt and salt-sensitivity contribute to cardiovascular disease. Distinct T cell phenotypic responses to high salt and hypertension as well as influences from environmental cues are not well understood. The aryl hydrocarbon receptor (AhR) is activated by dietary ligands, promoting T cell and systemic homeostasis. We hypothesized that activating AhR supports $CD4^+$ homeostatic functions, such as cytokine production and mobilization, in response to high salt intake while mitigating salt-sensitive hypertension. In the intestinal mucosa, we demonstrate that a high salt diet (HSD) is a key driving factor, independent of hypertension, in diminishing interleukin 17A (IL-17A) production by $CD4^+$ T (Th17) cells without disrupting circulating cytokines associated with Th17 function. Previous studies suggest that hypertensive patients and individuals on a high salt diet are deficient in AhR ligands or agonistic metabolites. We found that activating AhR augments Th17 cells during experimental salt-sensitive hypertension. Further, we demonstrate that activating AhR *in vitro* contributes to sustaining Th17 cells in the setting of excess salt. Using photoconvertible Kikume GreenRed mice, we also revealed that HSD drives $CD4^+$ T cell mobilization. Next, we found that excess salt augments T cell mobilization markers, validating HSD-driven T cell migration. Also, we found that activating AhR mitigates HSD-induced T cell migration markers. Using telemetry in a model of experimental salt-sensitivity, we found that activating AhR prevents the development of salt-sensitive hypertension. Collectively, stimulating AhR through dietary ligands facilitates immunologic and systemic functions amid excess salt intake and restrains the development of salt-sensitive hypertension.

Keywords: aryl hydrocarbon receptor, Th17, high salt diet, salt-sensitive hypertension, blood pressure

INTRODUCTION

High salt intake and hypertension are both significant factors leading to cardiovascular disease contributing to grave morbidity and a marked reduction in quality of life[1–4]. Economically, excess salt intake leads to the loss of tens of billions of dollars due to hospitalization and loss in productivity[5,6]. Thus, enumeration of mechanisms involved in high salt intake, with and without hypertension, is critical to US and global health. Environmental cues play a key role in regulating immune cell function and fate[7,8]. Studies have demonstrated distinct alterations in adaptive immunity, specifically effector $CD4^+$ T cells in response to high dietary salt[9–14] as well as in hypertension[15–18].

At homeostasis, Th17 cells are critical to maintaining health and function[19–23]. However, when homeostasis is disrupted, Th17 and IL-17A producing cells are known to promote various disease states, including hypertension[13,24–29]. Studies show that exogenous administration of interleukin 17A (IL-17A) further augments hypertension during angiotensin II-dependent hypertension [24,26], while other studies suggest that the loss of IL-17A abrogates end-organ damage during induced experimental hypertension[25,28]. Key studies show that Th17 cells are salt responsive with several mechanisms revealed[12–14,30]. Recent studies indicate that specific Th17 programs, aligned as homeostatic or pathogenic, may also influence cytokine production[29,31–33]. Previous work from Wu et al. and Matthias et al. identified a pathogenic phenotype of mouse and human Th17 cells in the context of high salt[14,30]. Homeostatic and pathogenic Th17 cells have been described in the gut and very little is known about how high salt intake affects the responses in homeostatic and pathogenic programming of Th17 cells.

The gut is highly responsive to changes in the diet and has the highest number of immune cells for all non-lymphoid tissues[34–36] making it a tissue of interest. Omenetti et al identified distinct homeostatic and pathogenic Th17 subsets in the intestines dependent on segmented filamentous bacteria (SFB) status with SFB having a specific effect on homeostatic Th17 cell differentiation[33]. Previous studies have shown that high salt intake promotes colitis

progression due to changes in the microbial environment and inflammation, however, the colonic pathogenic and homeostatic Th17 cell response to high salt was not reported[37,38]. Furthermore, mobilization and infiltration of $CD4^+$ effector T cells is central to end-organ pathogenesis across multiple diseases[31,39–44], but it is unclear if excess dietary salt directly impacts $CD4^+$ T cell mobilization. As the prevalence of excess dietary salt intake in today's society is high, further study is required to elucidate the mechanism(s) regulating homeostatic or pathogenic T cell functions by high salt[16,30,45–47].

The aryl hydrocarbon receptor (AhR) has been described as a key mediator of homeostatic Th17 responses[48–51]. AhR, which is ubiquitously expressed across diverse cell types[52], is critical for T cell function[53–55], and is highly dependent on ligand availability[48]. Numerous ligands enhance AhR activity with the most abundant dietary source derived from cruciferous vegetables[56]. Recent studies suggest that patients with hypertension and/or individuals who consume excess salt are deficient in tryptophan-derived indoles and AhR-binding metabolites[12,57,58]. AhR activation is also critical for protection against colitis[59]. However, it is unclear if reduced AhR activation is key to excess salt-responsiveness in Th17 cells or plays a role in salt-sensitive hypertension.

We, therefore, hypothesized that AhR activation in mice on a high salt diet and/or salt-sensitive hypertension supports $CD4^+$ homeostatic functions, specifically cytokine production and mobilization. We further hypothesized that loss of AhR activation contributes to salt-sensitive hypertension and that dietary supplementation of an AhR ligand mitigates salt-sensitive hypertension. To test these hypotheses, we employed an experimental model of salt-sensitive hypertension to evaluate the Th17 cell responses and blood pressure to high salt diet and/or salt-sensitive hypertension with AhR activation. We utilized a model of salt-sensitive hypertension, L-NAME+high salt diet to determine whether high salt diet alone is responsible for Th17 cell responses independent of augmented blood pressure or whether a systemic blood pressure response to HSD is required to disrupt Th17 cell functions. The pre-clinical L-

NAME/high salt experimental mouse model of salt-sensitive hypertension is widely used to recapitulate human salt-sensitivity.

Collectively, our study indicates that AhR activation in the presence of excess salt restores key facets of Th17 cell functionality and the homeostatic Th17 phenotype. Also, we show that the development of salt-sensitive hypertension is prevented with dietary supplementation to promote AhR activation. These pre-clinical studies would indicate that in the clinical setting activating AhR through dietary intervention may be a target in stabilizing $CD4^+$ T cell disruption in the setting of excess dietary salt consumption as well as restraining the development of salt-sensitive hypertension.

METHODS

Animal ethics. All animal and cellular experiments, derived from animals, were conducted following institutional, local, state, and federal guidelines. All permissions were provided by the Institutional Animal Care and Use Committee (IACUC) at the University of Alabama at Birmingham. All animals, unless indicated, were maintained in a humidity- and temperature-controlled room on a 12:12 hour lights on/off cycle (On 7 AM-7 PM; Off 7 PM-7 AM) with ad libitum access to food and water at the University of Alabama at Birmingham. Details about the diet and water are given below.

Mice. Specific-pathogen-free (SPF) C57BL/6J male mice were purchased from Jackson laboratory (Pathogen & Opportunist Free Maximum barrier facility RB10 with regular interval testing, Sacramento, CA) at weaning (18-21 days old). Jackson laboratory mice are devoid of segmented filamentous bacteria (SFB, *Candidatus Arthromitus*) while housed within the Jackson lab facilities[60–63]. Upon arrival at UAB, newly weaned 18-21-day-old mice were randomly assigned for co-housing to acquire UAB Kaul vivarium microbiome for at least 5 weeks and to normalize microbial composition across groups[64,65]. Following a 5-9-week

acclimatization period, in a random cohort of experimental C57BL6/J mice, 92% (11 of 12) tested PCR-positive for SFB and all tested PCR-negative for *Helicobacter hepaticus (Hh)*, indicating acquisition of SFB during the weaning reaction window. The Jackson laboratory confirms the use of a genomic stability program using monthly-introduced C57BL6/J founder mice into breeding colonies to minimize genetic drift. All mice entered experimental protocols between 8-12 weeks of age. IL17A-IRES-GFP-KI (IL-17A-eGFP) and Il17a^{Cre}R26R^{eYFP} (IL-17Afm-eYFP) fate-mapping mice were kindly provided by Dr. Laurie Harrington. Breeding pairs of CAG::KikGR (KikGR) photoconvertible mice were kindly provided by Dr. Troy Randall[66]. Littermate-matched male mice were utilized for all reporter colonies between 8-12 weeks of age. Where appropriate, tissues were collected during the inactive period between ZT1 and ZT3.

Diet. All diets were dye-free and matched nutritionally and provided ultra-filtered sterile (sterile) drinking water. Where indicated, mice were placed on a dye-free normal salt diet (NSD) (0.4% NaCl, TD.96208, Teklad) or nutritionally-matched high salt diet (4.0% NaCl, TD.92034, Teklad) plus 1% NaCl (wt/vol) sterile drinking water (HSD) for either 2-weeks or 5-weeks. Diets are identical in composition except for NaCl content. To investigate high salt diet-mediated blood pressure disruption, beginning between 8-12 weeks of age, mice were randomly assigned to the following groups: (a) NSD (TD.96208, Teklad) and sterile drinking water for the entire protocol, (b) NSD (TD.96208, Teklad) for 4-weeks followed by a two-week HSD period, or (c) provided NSD alongside L-NAME-supplemented sterile drinking water for three weeks followed by withdrawal of L-NAME and continued NSD and normal sterile drinking water for three weeks, or (d) mice were given NSD with 0.5 mg/mL L-NAME (Alfa Aesar; cat# AAH6366614) supplemented sterile drinking water for three weeks. Afterward, L-NAME was removed, and mice received NSD with normal sterile drinking water for 1 week. Following the 1-week hiatus, mice were then freely fed HSD for two weeks. L-NAME-supplemented sterile drinking water was

changed every third day, as previously described[12,67,68]. In specified experiments, Teklad directly incorporated indole-3-carbinol (I3C) into chow at 200 parts per million (mg I3C/kg chow)[69–71].

Photoconversion of Kikume GreenRed mice. Photoconversion procedures were adapted from protocols previously published and validated[66,72–76]. Kikume GreenRed male mice were anesthetized with 2% isoflurane (vol/vol) and maintained at 37℃ on a warming platform. Abdominal hair was shaved followed by the application of a depilatory cream for 2 minutes. Once the abdomen was cleared of all hair, a sterile environment was prepared with betadine surgical solution. A one-centimeter incision was made through the abdominal skin and abdominal wall. The small intestine with Peyer's patches was gently withdrawn with minimal disruption and laid onto a sterile aluminum foil blanket that covered the mouse to block and avoid light exposure to other tissues and lymph nodes. A Dymax QX4 405nm wand system with an LED head and collimator was placed 3.4cm above the withdrawn small intestine. The front and back of small intestinal tissue was exposed to 405nm light at an intensity of 95 mW/cm^2 for 13 minutes. During illumination, tissue was kept moist with sterile, warmed PBS. The intestine with Peyer's patches was returned to the abdominal cavity, followed by closure of the abdominal wall and skin with sterile suture. Mice were allowed to recover and provided analgesic therapy as directed and needed based on daily observation. Tissues were collected three days post-photoconversion to evaluate the presence of photoconverted KikumeRed$^+$ cells in tissues of interest, by flow cytometry, indicating immune cell egress from the small intestine. Ex vivo staining protocol below provides additional details for analysis by flow cytometry.

Preparation of tissues. All mice were anesthetized using an isoflurane aerosolizer with 1.5-2% isoflurane with the depth of anesthesia confirmed by gentle paw pressure. Blood was directly collected by cardiac puncture into an EDTA-coated syringe and centrifuged at 2,000G for 10min at 4℃ to separate plasma from red cell fraction. Plasma was immediately snap-frozen through

liquid nitrogen immersion followed by -80℃ storage until further analysis. Mice were then gently perfused with 10mL ice-cold PBS to remove blood-borne leukocytes in tissues. Tissue preparations for single-cell suspensions are described below.

Spleens and Lymph nodes. Spleens and lymph nodes were gently removed and crushed between two sterile frosted slides. Suspensions were filtered through 70 μm and 40 μm filters and centrifuged at 400g for 5min at 4℃. Splenocytes were ACK lysed, followed by quenching and re-centrifugation. Splenic and lymph node single-cell suspensions were resuspended in R10 and placed on ice until further processing[77,78].

Intestines and kidneys. The entire large intestine (without cecum) was harvested and cleaned of luminal contents and feces. Peyer's patches, from the distal two-thirds of the small intestine, were removed using curved scissors and placed into ice-cold R10 until processing. Intestines were cut into tissue segments followed by a quick wash with ice-cold buffer. Epithelial cells and intraepithelial lymphocytes were washed off by incubating in 37℃ stripping buffer (for 20 minutes at 200rpm on a flat-bottom shaker. Tissue pieces were transferred and resuspended in copious warm H2/wash buffer followed by mincing in 2mL R10. Minced tissue was digested at 37℃ at 200rpm in 10mL total digest buffer (1mg/mL collagenase type IV, 0.1U/mL dispase II, and 0.2 mg/mL DNase type I) for 45min followed by gentle disruption using a transfer pipette and gentleMACS dissociation (m_intestine_01). Enzymes were quenched with a large volume of ice-cold R5. Single-cell suspensions were filtered through 70 μm and 40 μm filters and centrifuged at 400g for 10min at 4℃. Kidneys were immediately collected, decapsulated and placed into 2mL complete media and minced. Subsequently, kidney pieces were digested (1mg/mL collagenase type IV, 0.1U/mL dispase II, and 0.2 mg/mL DNase type I) for 45min followed by gentle disruption using a transfer pipette and gentle MACS dissociation (non-lymphoid tissue program) and enzymes were quenched with a large volume of kidney wash buffer and filtered through 70 μm and 40 μm filters and centrifuged at 400g for 10min at 4℃. All

single cell suspensions were gently resuspended in 5mL 37% isosmotic percoll and centrifuged at 700g for 20min at 22℃ (acceleration 3, brake 0) to enrich colonic lamina propria lymphocytes (cLPL) and kidney immune cells. Debris was removed and the pellet was washed and centrifuged twice with ice-cold R10[79–81].

Peyer's Patches (PP). Isolated PPs were processed using the GentleMacs dissociator (m_spleen_02) followed by digestion in digest buffer (0.5mg/mL collagenase type IV, 0.1U/mL dispase II, 200μg/mL DNase type I) at 37℃ for 20min at 200rpm on a flat-bottom shaker. PP underwent GentleMacs dissociation (m_spleen_03) and mashed through a 70μm filter, followed by washing and filtering through a 40 μm filter. Samples were centrifuged at 400g for 7min at 4℃ and pellets were resuspended in R10.

Buffers. Complete RPMI media: RPMI-1640 supplemented with 2mM L- glutamine, 1% Pen-Strep, 50 μM 2-mercaptoethanol (2-ME), 1x NEAA, 10mM HEPES, 1mM Sodium Pyruvate, and 10% fetal bovine serum (FBS). Complete IMDM media: IMDM with 25 mM HEPES supplemented with 2mM L- glutamine, 1% Pen-Strep, 50 μM 2-ME, 1x NEAA, 1 mM Sodium Pyruvate, and 10% fetal bovine serum (FBS). H2/wash buffer: HBSS (w/o Ca/Mg), 2% FBS, and 1% Pen-Strep. Stripping Buffer (H2/EDTA/DTT): HBSS (w/o Ca/Mg), 5 mM EDTA, 1 mM dithiothreitol (DTT), 1% Pen-Strep, and 2% FBS. Kidney Wash buffer: HBSS (without Ca/Mg), 2% FBS, 2 mM EDTA. Flow cytometry (FACS) buffer: PBS (w/o Ca/Mg) with 2% FBS, 1% Pen-Strep, and 2 mM EDTA. Digestion buffer in R10: 1 mg/ml collagenase type IV (~285 U/mL), 0.1 U/mL dispase II, 200 μg/ml Deoxyribonuclease I from bovine pancreas (DNase I). R5: RPMI-1640 supplemented with 5% FBS, and 1% Pen-strep. Room temperature 37% Percoll in R5. Cell stimulation media: T cells: 50 ng/ml phorbol 12-myristate 13-acetate (PMA), 1 ug/ml ionomycin, 10 μg/ml Brefeldin A (BFA); ILC3: PMA/Ionomycin/BFA with 20 ng/ml recombinant mouse IL-1β and 20 ng/ml recombinant mouse IL-23. Fixation buffer: 2% PFA fixation buffer in FACS.

Catalog numbers. RPMI 1640 without L glutamine (SH30096FS, Fisher), HbSS without Ca, Mg, phenol Red (SH3058802, Fisher), Hyclone IMDM without glutamine (SH3025901, Fisher), PBS without Ca2+/Mg2+, Corning (MT21040CV, Fisher), Sodium Pyruvate (BW13-115E, Fisher), 100x non-essential amino acids (SH3023801, Fisher), HEPES (BP299100, Fisher), and 55mM 2-Mercaptoethanol in DPBS (21985023, ThermoFisher), Collagenase type IV, Gibco (17-104-019, Fisher), DNase Type I (DN25-100mg, Sigma), Dispase II (5U/mL), StemCell Tech (NC9886504, Fisher), EDTA, 0.5M, pH 8.0 (15-575-020, Fisher), Percoll (45-001-747, Fisher), Dithiothreitol, DTT (43819-5G, sigma), PMA (P1585-1MG, Sigma), Ionomycin, calcium salt, >98% (I0634-5MG, Sigma), eBioscience FOXP3 Kit (staining buffer kit Invitrogen™ 00552300) (50-112-8857, Fisher), Brilliant Violet buffer plus 1000T (BDB566385, Fisher), Ultra-comp beads (50-112-9040, Fisher) or Ultra-comp beads Plus (01-3333-42, ThermoFisher), Brefeldin A (B7651-25MG), 32% Methanol-free PFA.

Ex vivo stimulation. For intracellular cytokine determination, single-cell suspensions were stimulated with 50ng/mL phorbol myristate acetate (PMA), 1mg/mL ionomycin) at 37℃ in complete media for 1 hour. After 1 hour of incubation, brefeldin A (10ug/mL final concentration) was supplemented for the final 3 hours, at 37℃, to sequester cytokines. For ILC3 stimulations, stimulation media was supplemented with 20 ng/ml recombinant mouse IL-1β (130-101-682, Miltenyi Biotec), and 20 ng/ml recombinant mouse IL-23 (34-8231-82, eBioscience), in addition to PMA, Ionomycin, and brefeldin A protocol. Once complete, samples were spun down, stimulation media decanted, and washed twice with ice-cold FACS to quench stimulation[82].

Ex vivo staining. Single-cell suspensions were stained with amine-reactive live-dead dye (ThermoFisher amine-reactive live dead dye (live/dead aqua or live/dead blue) or Biolegend zombie near-infrared (NIR)) for dead cell exclusion in ice-cold PBS for 15 minutes protected from light at 4℃. After washing with cold FACS buffer, cells were incubated with Fc receptor

blockade (FcX plus and anti-CD16.2 FcγRIV) for 25 minutes followed by the addition of fluorophore-conjugated surface markers in ice-cold FACS (PBS, 2% FBS, 2mM EDTA) with brilliant violet plus buffer for an additional 25min on ice protected from light. Cells were washed and fixed overnight at 4℃ in FOXP3 eBioscience fixation buffer protected from light. Subsequently, samples were washed, and washed with room-temperature eBioscience FOXP3/transcription factor perm buffer, along with a brief 10 min incubation in perm buffer. Samples were then stained in permeabilization buffer for 45min at room temperature protected from light. Afterward, samples were washed and fixed in 2% PFA for 10min on ice protected from light. Samples were then washed twice, resuspended in cold FACS buffer, and protected from light at 4℃ until acquisition. In experiments with fluorescent reporter proteins, following surface staining, samples were gently fixed with 3.7% FA (Image-IT fixative, methanol-free) at room temperature for 20min. Cells were washed and permeabilized with 0.1% IGEPAL CA-630 for 4-5min at room temperature protected from light. Cells were washed twice with cold FACS and stained for intracellular cytokines overnight at 4℃ protected from light in FACS buffer. Samples were then washed twice, fixed, and resuspended in FACS. Samples were acquired on a BD FACSymphony A3/A5 flow cytometer or a Cytek Northern Lights spectral cytometer. In experiments where KikGR mice are used, KikGreen signal is detected using the 488nm laser (BP 515/20, LP 505), and KikRed signal is detected using the 561nm laser (BP 586/15, LP 570) on the BD FACSymphony A3/A5[83]. Flow cytometry data was analyzed with Flowjo software (V10, Tree Star). Single color controls were utilized to establish compensation and unmixing parameters (beads and cells), and fluorescence-minus-one (FMO), no-stimulation controls, and no-stain controls were utilized to assign gating. Dead cells and doublets were excluded from analysis and absolute cell counts.

Fluorophore-conjugated antibodies used for flow cytometry. CD45 (30-F11), TCRβ (H57-597), CD3 (145-2C11 or 17A2), TCR$\gamma\delta$ (GL3), CD4 (GK1.5), CD8α (53-6.7), CD25 (PC61),

CD11b (M1/70), CD11c (N418), CD44 (IM7), CCR6 (29-2L17), CXCR3 (CXCR3-173), IL-17A (TC11-18H10), IL-22 (IL22JOP or 1H8PWSR), Tbet (ebio4B10), FOXP3 (FJK-165), RORγt (AFKJ5-9), and IFNγ (XMG1.2). For ILC3 staining, biotinylated antibodies were used against CD11b (M1/70), CD11c (N418), TCRβ (H57-597), TCR$\gamma\delta$ (UC7-13D5), CD3ε (145-2C11), CD8a (53-6.7), CD8b (YTS156.7.7), F4/80 (BM8), Ter119 (TER-119), NK1.1 (PK136), KLRG1 (2F1), CD19 (6D5), Gr-1 (GR-1), then conjugated to streptavidin conjugated-PerCP-Cy5.5.

Isolation of naïve CD4$^+$ T cells. Mice were sacrificed and spleens were dissected and placed into sterile, cold R10. Spleens were crushed between two sterile fully frosted glass slides and filtered through 70 μm mesh. Red cells were ACK lysed, and the reaction was quenched with ice-cold MACS buffer, with single-cell suspension run through 40 μm filters. Samples were centrifuged followed by gentle resuspension. CD4$^+$ T cells were purified using CD4 (L3T4) microbeads according to manufacturer instructions (Miltenyi). Subsequently, the positively selected fraction was stained with fluorophore-conjugated antibodies to TCRβ, CD4, CD25, CD62L, and CD44. We sorted and collected naïve CD4$^+$ T cells (TCRβ^+CD4$^+$CD25$^-$ CD44^{lo}CD62L^{hi}) at the UAB Comprehensive Flow Cytometry Core using the BD FACS ARIA II cell sorter. In 96-well flat-bottom plates, 1-2x10^5 naïve CD4$^+$ T cells were cultured in complete R10 (L-glutamine-free RPMI-1640 supplemented with 2mM L- glutamine, 1% Pen-Strep, 50μM 2-ME, 1x NEAA, 10mM HEPES, 1mM Sodium Pyruvate, and 10% FBS). Using APC-free differentiation, we differentiated CD4$^+$ T cells under Th17 conditions using plate-bound αCD3ε and soluble αCD28. All cultures were split on day 3 and harvested on day 5. For homeostatic Th17 conditions, as defined by O'Shea, Kuchroo, Littman, and Weaver, among others[42,44,84,85], we stimulated cells with αCD3ε (2.5-10 μg/mL, as indicated), αCD28 (2 μg/mL), IL-6 (25 ng/mL), rhTGFβ1 (2 ng/mL), αIL-4 (10 μg/mL), and αIFNγ (10 μg/mL). For pathogenic Th17 conditions, as defined by O'Shea, Kuchroo, Littman, and Weaver, among others [42,44,84,85], cells were

stimulated with αCD3ε (10 μg/mL), αCD28 (2 μg/mL), IL-6 (25 ng/mL), IL-23 (20 ng/mL), IL-1β (20 ng/mL), αIL-4 (10 μg/mL), and αIFNγ (10 μg/mL). Where indicated, cultures were treated with 40 mM NaCl (Quality Biological), 100 nM FICZ (6-Formylindolo(3,2-b) carbazole, Enzo), 80 mOsm D-mannitol (Fisher Scientific), and untreated cultures were provided with the appropriate vehicle. αCD3ε (145-2C11), αCD28 (37.51), αIL-4 (11B11), and αIFNγ (XMG1.2) were purchased from Bio X cell. IL-6 (130-096-684), IL-1β (130-101-682), and rhTGFβ1 (130-095-067) were purchased from Miltenyi Biotec, and IL-23 (34-8231-82) was purchased from eBioscience (ThermoFisher Scientific). For cytokine determination, cultures were re-stimulated in 96-well U-bottom plates in complete media with 50ng/mL PMA and 1mg/mL ionomycin. After 1 hour of incubation, brefeldin A (B7651, Sigma) was supplemented for the final 3-hours to sequester cytokines. Cells were stained with amine-reactive live-dead dye, in cold PBS, to exclude dead cells, and stained for surface and intracellular markers as described above (using either eBioscience Foxp3 kit or BD Fix/Perm kit). Single color controls, fluorescence-minus-one (FMO), no-stimulation controls, and no-stain controls were utilized to establish compensation and unmixing parameters and gating, respectively.

Luminex multiplexed analyses. Plasma collected from mice was snap frozen by liquid nitrogen immersion followed by storage at -80℃. Once needed, plasma was thawed on ice. Following manufacturer instructions, plasma was analyzed for cytokines using the MT17MAG47K-PX25 Milliplex Luminex panel.

FITC-dextran gut-permeability assay. Mice are transferred to a new cage and fasted for 4 hours to limit coprophagy and access to chow. Mice are given 400mg/kg body weight FITC-dextran (3-5 kDa FD4, Sigma Aldrich) dissolved in water by oral gavage. Next, mice continue fasting for an additional 4 hours. Mice were anesthetized and 50-75 uL of blood is collected from the retro-orbital sinus. Blood collected is spun at 10,000 g for 10 minutes at room temperature

and the plasma is diluted 1:4 with water. Sample FITC-dextran concentration was analyzed with a spectrophotometer (excitation 485 nm, emission wavelength 528 nm). Plasma from a mouse given water by oral gavage was used to subtract background autofluorescence.

Telemetry. Telemetry devices (Data Sciences, PA-C10, St. Paul, MN) were implanted into the left carotid artery of isoflurane anesthetized mice. Mice were allowed to recover for 10 days before collection of baseline telemetry readings and subsequent dietary interventions. Recordings were obtained in 2-minute intervals every 10 minutes.

Segmented filamentous bacteria (SFB) and Hh (*Helicobacter hepaticus*) determination. Fecal pellets from a cohort of UAB-housed male 8-12-week-old C57BL6/J mice were collected into separate sterile microfuge tubes and immediately snap frozen. SFB and *Hh* colonization was qualitatively confirmed by analyzing DNA extracted from murine fecal pellets (fecal DNA extraction kit, Cat. No. D6010, Zymo Research) through PCR (SFB Primers: forward: 5'-ACGCTACATCGTCTTATCTTCCCGC-3', reverse: 5'-TCCCCCAAGACCAAGTTCACGA-3'; Hh Primers: forward 5'ATGGGTAAGAAAATAGCAAAAAGATTGCAA3', reverse: 5'CTATTTCATATCCATAAGCTCTTGAGAATC3').

Colonic tissue sodium content analysis. Colons were placed in nitric acid-cleaned ceramic crucibles, weighed, and desiccated for 48 hours in 75°C drying oven. Dried tissues were then weighed and the difference in weight prior to and after drying was considered water content as previously described[86]. Crucibles were then placed in a kiln for 40 hours at 450°C. After cooling, ash was reconstituted in 5% nitric acid and Na^+ content measured by atomic absorption (iCE 330 AAS, Thermo Fisher Scientific, Waltham, MA) and normalized to dry colon weight.

Statistical Analysis. Statistical analyses were performed with GraphPad Prism 9. Where appropriate and indicated, data was analyzed by paired or unpaired, two-tailed Student's t-test, ANOVA (one- and two-way), or two-way repeated-measures ANOVA. Data is plotted as mean±SEM. In cases in which non-normal distribution is found, appropriate non-parametric statistical analysis is completed (e.g., Mann-Whitney, etc.). Tukey's and Holms-Sidak multiple comparison's tests were carried out for post hoc analysis. $P<0.05$ was considered statistically significant. All data are pooled from, at least, 2-4 independent experiments, with each n indicating a biologically independent sample.

RESULTS

HSD depresses CD4$^+$ T cell cytokine expression

Three-week-old C57BL6/J males were purchased from Jackson Laboratory and accustomed to NSD and housed for 5-9 weeks, allowing them to acquire segmented filamentous bacteria (**Figure S1A**)[60–62]. Th17 cells and their cytokines, which include IL-17A and IL-22, are considered essential to homeostasis, found abundantly in the intestinal tract, and mediate host protection[87–89]. Therefore, as the intestinal luminal content contains high amounts of salt in mice and humans that consume a high salt diet, we sought to determine if excess dietary salt alone or in tandem with salt-sensitive hypertension predisposes CD4$^+$ T cells to produce IL-17A and IL-22. Thus, to evaluate the Th17 cell response to HSD, we fed mice either a normal salt diet (NSD) or a high salt diet (HSD). Further, we induced experimental salt-sensitive hypertension by conditioning mice with N(gamma)-nitro-L-arginine methyl ester (L-NAME), pan-nitric oxide synthase inhibitor, followed by feeding with HSD alone, recapitulating salt-sensitive hypertension [67,68]. Some experiments include conditioning with L-NAME followed with NSD fed mice to inform whether systemic nitric oxide synthase inhibition and short-term rise in blood pressure may be involved in Th17 cell disruptions. As HSD feeding alone does not promote a rise in blood pressure in C57BL6/J mice[90,91], the experimental salt-sensitive

hypertension model informs whether HSD alone is responsible for Th17 cell responses independent of augmented blood pressure or whether a systemic blood pressure response to HSD is required to disrupt Th17 cell functions (**Figure 1A**).

We interrogated the expression and population abundance of IL-17A- and IL-22-expressing $CD4^+$ T cells in the colons of NSD-fed mice, HSD-fed mice, L-NAME-conditioned mice fed NSD, or L-NAME-conditioned mice fed a HSD (salt-sensitive mice). Using the gating scheme shown in **Figure S1B,** we determined the abundance of IL-17A- and IL-22-expressing $CD4^+$ T cells in the colons of the four groups. We found that $CD4^+$ IL-17A and IL-22 were markedly reduced in HSD-fed mice, with parallel responses by L-NAME-conditioned mice fed NSD, and salt-sensitive mice fed a HSD compared to NSD fed control mice (**Figure 1B**). These findings show that Th17 cells are sensitive to excess salt diet as well as a short-term rise in blood pressure. Total $CD45^+$ and $CD4^+$ T cell cLPL compartments were unaffected in HSD-fed, L-NAME-conditioned mice fed NSD, or salt-sensitive mice, suggesting a specificity for Th17 cells by excess salt diet and L-NAME conditioning (**Figure S2A**). The pro-inflammatory $CD4^+$ T cell population, IL-$17A^+TNF\alpha^+CD4^+$ T cells, was blunted in response to excess salt diet and in salt-sensitive mice, however no significant difference was found in L-NAME-conditioned mice fed NSD (**Figure S2B**). Thus, suggesting that pro-inflammatory Th17 cells are sensitive to excess salt diet but not a rise in blood pressure.

Since Th17 cells can contribute to intestinal homeostasis[33,92,93], we reasoned that the experimental salt-sensitive mice may have altered colonic permeability. Indeed, we observed that salt-sensitive mice had significantly increased colonic permeability to FITC-dextran compared to NSD mice (**Figure S2C**). Many investigations have previously shown that HSD increases gut absorption of salt[94], acute elevations in plasma sodium[95,96], and increased excretion of urinary sodium[97,98]. We confirmed that sodium content in colonic tissue from HSD and L-NAME/HSD mice was elevated in the colon compared to NSD mice (**Figure S2D**).

Collectively, these data indicate that salt-sensitivity is associated with reduced colonic Th17 cells, increased colonic permeability, and higher colonic sodium content.

Further, we assessed responses of retinoic acid-related orphan receptor gamma t^+ (RORγt^+) $Foxp3^-CD4^+$ T cells as well as forkhead box protein P3 $(Foxp3)^+$ $CD4^+$ T regulatory cells, and T-box transcription factor TBX21 $(T\text{-}bet)^+CD4^+$ T cells to excess salt diet and in salt-sensitive mice to determine the specificity of the Th17 response. RORγt^+ is the master transcription factor for Th17 cells[99]. As expected, we found that ROR$\gamma t^+Foxp3^-CD4^+$ T cells were decreased by excess dietary salt, L-NAME-conditioned mice fed NSD, and in salt-sensitive mice (**Figure S3A**), in agreement with the Th17 cell response. Whereas, $Foxp3^+CD4^+$ T regulatory cells and $T\text{-}bet^+CD4^+$ T cells remained stable and were unaffected in all groups of mice (**Figure S3A, S3B**). Finally, Type 3 innate lymphoid cells (ILC3) were also unaffected in all groups of mice (**Figure S3C**). Thus, these observations further validate the specificity for the Th17 cell response to high dietary salt and salt-sensitivity.

We examined whether longer HSD feeding for 5 weeks would elicit a similar Th17 response as 2 weeks. Colonic IL-17A and IL-22 expressing $CD4^+$ T cells were also decreased in response to 5-weeks of HSD, suggesting that acute and longer-term consumption of HSD promotes contraction of the Th17 cell pool without an apparent pro-inflammatory switch (**Figure 1C**). We also assessed whether the Th17-associated cytokines IL-17A, IL-22, GM-CSF, and TNFα were disrupted by excess salt diet and experimental salt-sensitive hypertension. We found that circulating IL-17A, IL-22, GM-CSF, and TNFα were unchanged by HSD, L-NAME-conditioned mice fed NSD, or salt-sensitive mice (**Figure 1D**) suggesting that these HSD responses are stable and most likely are not systemically mediated.

We determined whether the naïve $CD4^+$ T cell compartment is sensitized to salt-sensitivity *in vitro.* We utilized naïve $CD4^+$ T cells isolated from NSD-fed and salt-sensitive mice, polarized them under Th17-polarizing conditions in the presence or absence of additional NaCl in the cell media. Polarized Th17 cells from NSD-fed and salt-sensitive mice both had

decreased IL-17A production in response to excess salt *in vitro*, indicating that the induced IL-17A T cell program remained stable among the naïve CD4 compartment (**Figure 1E**). Peyer's patches serve as key site for priming $CD4^+$ T cells and for sensing luminal contents along the intestinal tract[100–104]. Therefore, we utilized the IL-$17^{fm/eYFP}$ fate-mapping mouse[103] and sought to confirm that HSD directly disrupts Th17 cells in Peyer's patches, a key immunologic priming site. In concert with colonic and *in vitro* data, HSD reduced the $Th17^{efm/eYFP}$ pool found in Peyer's patches (**Figure 1F**). Taken together, we established that HSD depresses IL-17A and IL-22 expression by $CD4^+$ T cells among the intestinal mucosa, in the absence of circulating cytokine perturbations[74,105–107].

At homeostasis, Th17 cells have an enriched non-pathogenic signature, which includes expression of the aryl hydrocarbon receptor (AhR), an established trans-activator of IL-17A among $CD4^+$ T cells. Using next-generation RNA-sequencing published by Matthias et al.[14], we evaluated unexplored candidate genes among polarized human Th17 cells exposed to high and normal salt. We specifically focused on candidate genes involved in T cell stability, AhR metabolite response, and migration. CYP1A1 (Cytochrome P450, family 1, subfamily A, polypeptide 1) catabolizes AhR ligands[108] suggesting that an imbalanced CYP1A1:AhR presence would lead to decreased AhR ligands. We noted that exposure to high NaCl *in vitro* led to an increased CYP1A1:AhR ratio in Th17 cells (**Figure 1G**). Further, we observed a significant increase in the expression of CCR6 and CXCL10 (C-X-C Motif Chemokine Ligand 10), a key ligand for CXCR3[109,110], with marked depression in CXCR6, a key pathogenic marker, in Th17 cells exposed to high salt conditions (**Figure 1G**). Analysis of key regulatory pathways show increased negative regulation of cell-cell adhesion, augmented cell migration programs, and reduced cytokine signaling pathways (**Figure 1H**). These data indicate that excess salt links human T cell programs leading to increased mobilization and disrupted cytokine expression.

AhR activation promotes Th17 expansion during excess salt intake and exposure

Recent work has demonstrated that AhR activating ligands are depleted in patients that consume a high salt diet or display hypertension, and salt-sensitive animal models have further validated these observations[12,57]. As AhR is involved in promoting IL-17A expression[111,112], we reasoned that reduced AhR ligand availability or decreased AhR activation may be responsible for blunted Th17 cell abundance. We assessed whether activating AhR in the setting of salt-sensitive hypertension promotes IL-17A-expressing $CD4^+$ T cells *in vivo* and *in vitro*. L-NAME conditioned mice were either given HSD chow or HSD chow supplemented with the AhR activator indole-3-carbinol (I3C)[71] followed by evaluation of the Peyer's patch Th17 compartment to examine whether the Th17 compartment was augmented in AhR-activated HSD-fed mice (**Figure 2A**). We observed in the mice fed the HSD+I3C chow an expansion of Th17 cells among the Peyer's patch compartment with augmented expression of CD69, a marker of early activation and mobilization arrest (**Figure 2B**). We next assessed if this expansion was a function of cellular proliferation by examining the expression of Ki-67, a marker of active proliferation. Interestingly, Ki-67 was not augmented in mice with the AhR-activating chow indicating that the IL-17A program is upregulated independent of cellular proliferation (**Figure 2B**). Importantly, these data indicate that activating AhR through dietary ligands represents a physiologic stimulus for expanding non-pathogenic Th17 cells among priming sites.

Th17 cells can generally be classified as homeostatic or pathogenic based on their differentiation pathway and functional phenotypes[78]. We designed *in vitro* studies to determine if directly activating AhR with 6-Formylindolo(3,2-b) carbazole (FICZ)[113,114] upregulates IL-17A among excess salt-treated homeostatic or pathogenic Th17 cells (**Figure 2C**). Consistent with our earlier observations, increased NaCl reduced IL-17A among $CD4^+$ T cells under homeostatic polarizing conditions (**Figure 2D**). In contrast, naïve $CD4^+$ T cells polarized under pathogenic

conditions showed an expanded IL-17A response to increased NaCl (**Figure 2D**). To determine a direct effect of NaCl or a change in osmolality on polarizing Th17 cells under homeostatic or pathogenic conditions, we treated polarizing cells with mannitol, an osmotically active agent. Th17 cells polarized under homeostatic conditions were non-responsive to mannitol treatment, yet under pathogenic conditions Th17 cells were expanded. Thus, indicating a clear dichotomous response that homeostatic Th17 cells are sodium-dependent whereas pathogenic Th17 cells are osmotic-dependent (**Figure 2D**). Further studies are needed to determine the molecular mechanisms dictating these distinct responses.

Activating AhR in these homeostatic polarizing conditions even in the presence of excess NaCl promoted IL-17A expression (**Figure 2D**). Thus, suggesting that AhR responsiveness remains intact in homeostatic cultures despite excess salt conditions. However, naïve $CD4^+$ T cells polarized under pathogenic conditions showed an expanded IL-17A in response to increased NaCl but lacked an AhR response (**Figure 2D**) confirming that the AhR program is inactive in Th17 cells polarized under pathogenic conditions. Taken together, these data suggest that activating AhR selectively expands homeostatic Th17 cells while limiting pathogenic Th17 cell activity. To further confirm regulation of IL-17A expression in the presence of AhR activation, we employed the IL-$17A^{fm/eYFP}$ fate mouse and polarized naïve $CD4^+$ T cells under homeostatic and pathogenic conditions and determined if activating AhR regulated IL-$17A^{fm/eYFP}$ expression (**Figure 2E**). In agreement with our previous findings, Th17 cell fate was augmented in response to AhR activation with high salt exposure under homeostatic conditions (**Figure 2F**). Th17 cells polarized under pathogenic conditions were expanded in response to salt without additional IL-17A expression following AhR activation (**Figure 2F**). These *in vitro* data further validate key programmatic differences between homeostatic and pathogenic Th17 cells, with AhR activity being enriched among homeostatic Th17 cells.

Activating AhR regulates mobilization induced by HSD in $CD4^+$ T cells

Key studies demonstrate that AhR activation also regulates immune cell mobilization[115,116]. Since we found that AhR activation regulates IL-17A expression *in vivo* and *in vitro* during excess salt conditions, we reasoned that activating AhR may regulate $CD4^+$ T cell migration markers under high salt exposure. First, we examined whether the naïve $CD4^+$ T cell compartment in NSD or salt-sensitive mice was primed with respect to expression of CXCR3[110], a key migration marker among $CD4^+$ T cells, during Th17 cell differentiation by *in vitro* experiments. We utilized naïve $CD4^+$ T cells isolated from NSD-fed and salt sensitive mice, polarized under homeostatic conditions in the presence or absence of excess NaCl (40mM) in the cell media. Homeostatic Th17 cells from NSD-fed and salt sensitive mice both responded to excess salt in which we observed upregulation of CXCR3 among Th17 cells *in vitro* (**Figure 3A**). Interestingly, Th17 cells from salt-sensitive mice had a significantly enhanced response to excess salt than the Th17 cells from NSD fed mice (**Figure 3A**). We also examined whether CCR6[117,118], another key migration marker, would be upregulated in response to high salt under homeostatic Th17-polarizing *in vitro* conditions (**Figure 3B**). We observed that CCR6 expression was upregulated in Th17 cells isolated from either NSD-fed or HSD-fed mice when exposed to excess salt and the response from HSD-fed mice was significantly higher than from NSD-fed mice *in vitro* (**Figure 3B**). We next examined whether the migration marker, CXCR3, was upregulated in Th17 cells from HSD fed mice *in vivo* (**Figure 3C**). Similarly, we found upregulation of CXCR3 among fated Th17 cells in the Peyer's patches of HSD-fed mice (**Figure 3C**). These findings suggest that high salt directly reprograms mobilization potential for egress from the Peyer's patches, thus, further studies determined the $CD4^+$ T cell migration with HSD from the small intestine/Peyer's patches.

We employed the CAG::KikGR[33] transgenic mouse model, which expresses the photoconvertible fluorescent reporter protein, Kikume Green-Red(KikGR)55, to substantiate the HSD-induced CD4+ T cell migration from the small intestine to extra-intestinal sites. Upon illumination with 405 nm light, the KikGR protein undergoes irreversible photoconversion from its native green state to a red isoform (KikGreen to KikRed) which allows for cell tracking (**Figure 3D**). Furthermore, photoconversion is limited to tissues illuminated allowing for specific control in tissue-specific mobilization and does not photoconvert circulating immune cells nor tissue protected by the sterile aluminum shield (**Figure S4A**). We examined if mice fed 5 weeks of HSD promotes small intestinal (including Peyer's patches) $CD4^+$ T cell egress to mucosal and non-mucosal associated tissues. Intriguingly, HSD increased the presence of $KikRed^+$ $CD4^+$ T cells in the mesenteric lymph node, mLN, colonic lamina propria, cLP, and pooled caudal/iliac LN, all key mucosal-associated tissues (**Figure 3E**). The mLN and caudal/iliac LN specifically drain sites within the colon. Whereas the frequency of $KikRed^+$ $CD4^+$ T cells remained stable with 5-weeks of HSD in the inguinal LNs (ingLNs), spleen, kidneys, and whole blood (all non-mucosal-associated tissues) (**Figure S4B**). Whether Th17 cells are the primary $CD4^+$ T cell subset that is migrating remains to be determined. Regardless, these data provide a proof of concept that HSD stimulates $CD4^+$ T cell migration between mucosal tissues. Altogether, excess salt exposure *in vitro* and HSD *in vivo* sensitizes and promotes $CD4^+$ T cell migration as evidenced by upregulation of key migration markers and migration to remote mucosal-associated tissues.

We sought to determine if activating AhR reprograms $CD4^+$ T cell migration markers altered by HSD. We reasoned that activating AhR may blunt the expression of CXCR3 and CCR6 under high salt conditions among $CD4^+$ T cells. We utilized polarized naïve $CD4^+$ T cells under homeostatic and pathogenic Th17 *in vitro* conditions in the presence of high salt or high salt coupled with the AhR activator, FICZ (**Figure 3F**). Indeed, activating AhR with FICZ under high salt conditions normalized the frequency of CXCR3 expressing Th17 cells exposed to high

salt under homeostatic conditions (**Figure 3F**). In contrast, neither high salt nor AhR activation with FICZ affected CXCR3 expressing Th17 cells under pathogenic conditions (**Figure 3F**). These findings further validate a role for AhR in homeostatic Th17 function in the context of high salt.

To further confirm AhR activation as a regulatory focus for effector $CD4^+$ T cells under high salt conditions, naïve $CD4^+$ T cells were isolated from mice fed 2 weeks of NSD or HSD and polarized under homeostatic and pathogenic conditions with excess salt in the absence or presence of FICZ *in vitro* (**Figure 3G**) and examined whether CCR6 expression was regulated under these conditions. We found that 2-weeks of HSD led to increased $CCR6^+$ homeostatic Th17 cells compared to mice fed a NSD (**Figure 3G**). Interestingly, both NSD and HSD fed mice saw an increase in $CCR6^+$ homeostatic Th17 cells with excess salt in the media that was attenuated with FICZ treatment (**Fig 3G**) In contrast, Th17 cells polarized under pathogenic conditions did not demonstrate regulation of CCR6 expression with AhR activation. Taken together these findings indicate that activating AhR may offer a physiological avenue to limit inappropriate $CD4^+$ T cell egress from the gut by blunting migration in response to excess salt.

AhR activation blunts the development of salt-sensitive hypertension

Foundational studies demonstrate control of blood pressure by immune cells, and notably T cells[45,119]. However, whether AhR activation plays a key role in salt-sensitive hypertension is not established. We examined if activating AhR supplants HSD-dependent increased blood pressure in a mouse model of salt-sensitivity. We provided HSD without or with the diet-derived, high-affinity AhR pro-ligand indole-3-carbinol (I3C) to L-NAME conditioned salt-sensitive mice and evaluated the blood pressure response by telemetry (**Figure 4A**). All mice displayed a diurnal rhythm in blood pressure and heart rate (**Figure 4B-4I**) with averages of light and dark periods denoted by the alternating white and gray areas. As expected, mice fed chow with HSD after L-NAME conditioning displayed increased salt-sensitive hypertension, as

observed with significantly elevated mean arterial, systolic, and diastolic blood pressure (MAP, SBP, and DBP, respectively) during the light and dark periods (**Figure 4B-4G**). Interestingly, we found that mice fed chow with HSD supplemented with the AhR activator I3C after L-NAME conditioning did not develop salt-sensitive hypertension and showed a salt-resistant blood pressure phenotype (**Figure 4B-4G**) but without an alteration in heart rate (**Figure 4H-4I**). It is known that metabolism of AhR ligands, specifically I3C, occurs in the intestine with limited I3C-derived metabolites found systemically[70]. While more research is needed, these findings suggest that the control of salt-sensitive hypertension by AhR-activating ligands may be limited to the intestinal tract.

DISCUSSION

Here we demonstrate that activating AhR directs homeostatic Th17 cells amid excess salt as well as restrains the development of experimental salt-sensitive hypertension. Our study unraveled novel non-canonical salt-sensitive $CD4^+$ T cell responses highlighting a central role for AhR in blunting the salt-sensitive Th17 cell fate. Th17 cells have extreme plasticity, and the environment determines their homeostatic or pathogenic fate[33]. Distinct homeostatic Th17 cells are present in the intestine as well and are critical for barrier integrity[33,120,121]. While several groups have defined a pathogenic phenotype of Th17 cells that is present in the intestine with an increase in IL-23 signaling[121,122]. Our study found that direct AhR activation in polarized homeostatic and pathogenic Th17 cells show divergent responses to high salt analogous to *in vivo* conditions. We also discovered salt-responsive $CD4^+$ T cell mobilization as well as increased expression of migration markers with high salt both *in vivo* and *in vitro* conditions. AhR activation in the presence of excess salt leads to blunted migration marker expression specifically in homeostatic Th17 cells. Furthermore, our study revealed that AhR activation via dietary supplementation with I3C blocks the development of experimental salt-sensitive

hypertension. In summary, activating AhR fosters homeostatic control of effector $CD4^+$ T cells in the presence of excess salt and prevents the development of salt-sensitive hypertension.

Numerous mechanisms have been proposed as cooperative factors in the response to excess dietary salt and salt-sensitive hypertension[123–125]. Several contrasting studies have demonstrated that excess dietary salt does not elicit an inflammatory response or may lead to immunosuppression[24,126]. Kleinewietfeld et al. and Wu et al., published seminal studies outlining a role for excess salt in promoting Th17 cells in mice with induced myelin oligodendrocyte glycoprotein (MOG) peptide 35-55 (MOG_{35-55})-dependent experimental autoimmune encephalomyelitis (EAE), a mouse model of multiple sclerosis[13,30]. Wilck et al., elegantly demonstrated an association between the Th17 compartment expansion amidst salt-sensitive hypertension[12] and Madhur and colleagues show a role for IL-17A to worsen hypertension[24–26,28]. While our study found mucosal Th17 cell contraction in response to HSD and salt-sensitive mice, the murine strain differences or microbiota differences may underlie the potential discrepant study results. Notably, Wilck et al., used specific pathogen-free/virus antibody-free FVB/N mice acquired from Charles River at 12 weeks of age [12], while our study used 8-12-week-old C57BL6/J mice from Jackson laboratory acquired at 3 weeks old, which were subsequently colonized with SFB during the post-weaning reaction window. Indeed, Robertson et al show the importance of acclimatization protocols and breeding strategies to standardize microbiota for reproducible results[127]. Thus, differences in the murine genetic background and microbial imprinting between our study and the previous reports, may explain the key discrepancies[128–131].

We observed that the *in vivo* response to a high salt diet is reflected in the *in vitro* response with Th17 cells cultured under homeostatic conditions (TGFβ and IL-6). Ghoreschi et al., and others have elegantly demonstrated key programmatic differences between homeostatic (or protective) and pathogenic Th17 cells[132–134]. Among homeostatic Th17 cells,

AhR activation was enriched whereas pathogenic Th17 cells show prominent T-bet induction[43,44]. Therefore, we hypothesized that activating AhR may expand Th17 cells despite high salt conditions. Indeed, *in vitro* and *in vivo* AhR activation in the presence of high salt promoted Th17 cells. Recent clinical trials evaluating the efficacy of anti-IL-17A treatment in patients with colitis noted local and systemic clinical deterioration, presumably through disruption of local indispensable Th17-dependent homeostatic mechanisms[21,33]. Homeostatic Th17 cells were identified in the intestines and are studied in their role related to the intestinal barrier. [33,120] In line with these studies, we found that the L-NAME-induced model of salt sensitivity showed increased intestinal permeability as well as higher sodium content in the colon. However, identifying a role for homeostatic Th17 cells in other organs and tissues is yet to be described. Thus, further research is needed to determine whether homeostatic Th17 cells play a role in blood pressure responses to dietary interventions.

Key facets of T cell function, such as mobilization and cytokine expression, and how these are influenced by excess salt are not well-established[18]. We found that small intestinal-derived $CD4^+$ T cells migrate in response to high salt suggesting disruption of homeostasis. *In vitro* models corroborated that excess salt heightens $CD4^+$ T cell function and migration directly. Interestingly, multiple groups have demonstrated that autoimmune experimental models promote migration of small intestine-derived $CD4^+$ T cells[135]. We also demonstrate that effector $CD4^+$ T cells upregulate the canonical migration marker CXCR3, *in vitro* and *in vivo*, with high salt. Intriguingly, the population of $CD4^+$ T cells fated to express IL-17A is reduced in Peyer's patches. Using varied *in vitro* conditions, we found that specific T cell priming conditions dictate responsiveness to excess salt and AhR activation. Specifically, a reduction in CXCR3 following AhR activation suggests sustained homeostatic Th17 programs. In brief, when excess salt is present in the diet or in cell culture conditions, $CD4^+$ T cells are primed to mobilize with tandem inactivation of the IL-17A program. Intriguingly, the loss of IL-17A and increased CXCR3 among

$CD4^+$ T cells may reflect the reprogramming of pathogenic ex-Th17 cells[78]. Collectively, this study provides primary evidence for HSD-induced migration of intestinal-derived $CD4^+$ T cells.

Matthias et al. revealed key differences in the response to high salt between human induced homeostatic and pathogenic Th17 cell fates[14]. Using the Matthias database of human transcriptomics with single-cell RNA-sequencing, we identified Th17 candidate genes that approximate the murine responses to excess salt found in our study. For example, increased CCR6 and CXCL10 with reduced CXCR6 may reflect preponderance to mobilize with high salt. Further, an augmented CYP1A1:AhR ratio in human Th17 cells exposed to high salt may indicate decreased AhR ligand availability for Th17 stability due to CYP1A1-dependent ligand metabolism[136,137].

Critical studies yielded that exogenous administration of IL-17A augments blood pressure[24,26], whereas, in some cases, infusion with anti-IL-17A did not reduce blood pressure[138]. Subsequently, Krebs and Lange et al. demonstrated that loss of IL-17A and IL-23 accelerates end-organ injury in deoxycorticosterone acetate + angiotensin II-induced hypertension[17,138]. L-NAME-induced salt-sensitive hypertension, which presents with lower circulating angiotensin II levels, is distinct from angiotensin II-dependent hypertension with divergent mechanistic underpinnings[139,140141]. Harrison's laboratory first demonstrated a linkage between L-NAME-induced salt-sensitive hypertension and increased non-lymphoid Th17 cells[68]. Our study, however, finds blunted Th17 cell responses in the colon with L-NAME induced salt sensitive hypertension as well as with high salt only and L-NAME conditioning. Our study focused on the mechanisms of how high salt conditions influence Th17 cell differentiation and activation. It is interesting that L-NAME conditioning itself has a significant effect on Th17 cells, however we focused on the high salt and salt-sensitive dependent mechanisms. Thus, a limitation of our study is the lack of understanding whether L-NAME conditioning and high salt diet work through the same mechanism affecting the Th17 cell fate.

Overall, our current work highlights the diversity and complexity of Th17 responses, especially with regards to AhR activation, in the presence of high salt and in the development of salt-sensitive hypertension. These data show that AhR activation via dietary supplementation with I3C reduces blood pressure in an L-NAME-induced salt sensitive model. Several investigations[142–144] show distinct differences in the systemic activation of AhR by I3C or when AhR activation is limited to the intestine with dietary I3C supplementation similar to our study. During digestion, I3C is metabolized into AhR ligands. I3C-supplemented diet in the non-obese type 1 diabetic mouse model, NOD mice, lead to strong AhR activation in the small intestine but minimal systemic AhR activity[142]. Dietary I3C did not alter T helper cell differentiation in the spleen or pancreatic draining lymph nodes. However, dietary I3C increased the percentage of $CD4^{+}ROR\gamma t^{+}Foxp3^{-}$ (Th17 cells) in the lamina propria, intraepithelial layer, and Peyer's patches of the small intestine of NOD mice. The immune modulation in the gut was accompanied by alterations to the intestinal microbiome, with changes in bacterial communities observed within one week of I3C supplementation[142]. Our study indicates a potential role of colon-derived Th17 cells associated with driving the blood pressure response, however, these data are not conclusive. Although, it is tempting to speculate that a basal reservoir of Th17 cells within the intestinal compartment is required and indispensable for local homeostasis and potentially systemic blood pressure regulation. Further research will test the hypothesis that the activation of AhR in the colon is driving the blood pressure response.

In conclusion, these findings show that in the setting of experimental salt-sensitivity, activating AhR promotes T cell stability and controls the sensitivity of blood pressure response. Experimentally, the deletion of AhR in mice seems an obvious model to study the relationship between AhR and salt-sensitive hypertension. However, the absence of AhR, systemically or cell-specific, leads to deleterious physiological consequences. For example, loss of $CD4^{+}$ T cell-specific AhR leads to disruption in the Th17 differentiation, inability for Th17-transdifferentiation, and inability to sustain epithelial integrity[145]. Deletion of AhR among epithelial cells results in

intestinal epithelial stem cell disruption leading to unrestricted proliferation and impaired differentiation[146–148]. Myeloid-specific AhR deletion leads to inappropriate intestinal morphogenesis, epithelial differentiation and decreased epithelial integrity[116]. Studying salt-sensitivity through constitutive AhR knockout mouse models would most likely be confounded by these physiological consequences. The pathogenesis of salt-sensitivity is not restricted to adaptive immune mechanisms but also rely on renal, endothelial and/or neural signaling. Thus, cell-specific inducible AhR knockout mouse models would be a valuable tool for future research efforts.

Perspectives

Blunting salt-sensitive hypertension through specific dietary modifications is sought after clinically. Guidance by the American Heart Association Life's Essential 8 recommends sustained intake of vegetables, such as broccoli, which are enriched in AhR activating ligands[6]. Clinically, the recent generation of designer indoles with high affinity and high potency for AhR in therapeutic ranges provides a promising tool in targeting intestinal disruptions, hypertension, and immune cell dysfunction[149]. Overall, this work provides evidence that increasing high-affinity AhR ligand availability provides a diet-based therapeutic platform to minimize mucosal disruption as well as reduce the hypertensive response to excess dietary salt intake.

Acknowledgments

We appreciate the efforts of Vidya Sagar Hanumanthu, Associate Director of the UAB Flow Cytometry and Single Cell Core. We also gratefully acknowledge the scientific discussions and technical assistance by Ryan McMonigle. Further, the UAB/UCSD O'Brien Core Center for Acute Kidney Injury Research provided excellent surgical support with telemetry implantation.

Author Contributions

P.A.M, C.J.E., C.L.M., and J.S.P. designed and contributed to experimental analysis with input from C.D.M., A.A.B., L.E.H., D.M.P., and D.N.M. P.A.M., C.J.E., L.S.D., C.E.K., R.Q.M., M.S.J., D.B., and M.K.R. carried out experiments. P.A.M., J.C.C., M.K.R., D.M.P., and J.S.P. involved in conceptualizing telemetry experiments and animal colony management. S.M.P. and T.D.R. provided training and KikGR mouse model with conceptual support and guidance. P.A.M., C.J.E., A.A.B., L.E.H., C.L.M., D.N.M., and J.S.P. involved in conceptualizing culture experimental systems. All authors approved the manuscript.

Funding

This research was supported by F31HL151264, T32DK116672, and T32GM8361 to P.A.M., F31HL167626, T32GM811135, and TL1TR003106 to C.J.E., F31HL149235 to L.S.D., K01HL145324 to C.D.M.; F31HL165863 to C.E.K., R01DK125870 to L.E.H., TL1DK139566 to M.K.R., Deutsche Forschungsgemeinschaft (DFG, German Research Foundation) Projektnummer 394046635-SFB 1365 and DFG-SFB1470/ A06, by the Deutsches Zentrum für Herz-Kreislauf-Forschung (DZHK, 81Z0100106) and by the BMBF (The Federal Ministry of Education and Research), Foerderkennzeichen 01EJ2202D (TAhRget consortium) to D.N.M.; R01DK118386 to C.L.M.; CCF Research Initiatives Award 558420 to C.L.M. and J.S.P., P01HL136267, P01HL158500, and R01DK134562 to D.M.P. and J.S.P.

Disclosures

DMP holds the position of Editor-in-Chief of *FUNCTION* and is blinded from reviewing or making decisions for the manuscript.

References

1. Yoon H, Cai Q, Yang JJ, et al. Sodium Intake and Cause-Specific Mortality Among Predominantly Low-Income Black and White US Residents. *JAMA Network Open.* **7,** e243802 (2024).
2. Cook, N. R., Appel, L. J. & Whelton, P. K. Sodium Intake and All-Cause Mortality Over 20 Years in the Trials of Hypertension Prevention. *Journal of the American College of Cardiology* **68,** 1609-1617 *(*2016).
3. Zhou, D., Xi, B., Zhao, M. *et al.* Uncontrolled hypertension increases risk of all-cause and cardiovascular disease mortality in US adults: the NHANES III Linked Mortality Study. *Sci Rep* **8**, 9418 (2018).
4. Zhou, B., Perel, P., Mensah, G. A. & Ezzati, M. Global epidemiology, health burden and effective interventions for elevated blood pressure and hypertension. *Nature Reviews Cardiology* **18**, 785–802, (2021).
5. Lerman LO, Kurtz TW, Touyz RM, *et al.* Animal Models of Hypertension: A Scientific Statement From the American Heart Association. *Hypertension* **73**, e87–e120, (2019).
6. Lloyd-Jones DM, Allen NB, Anderson CAM, *et al.* Life's Essential 8: Updating and Enhancing the American Heart Association's Construct of Cardiovascular Health: A Presidential Advisory from the American Heart Association. *Circulation* **146**, E18–E43 (2022).
7. Tuong, Z. K., Stewart, B. J., Guo, S. A. & Clatworthy, M. R. Epigenetics and tissue immunity—Translating environmental cues into functional adaptations. *Immunological Reviews* **305**, 111–136, (2022).
8. Stockinger, B. T cell subsets and environmental factors in Citrobacter rodentium infection. *Curr Opin Microbiol* **63**, 92–97 (2021).
9. Hernandez, A. L. Kitz A, Wu C, *et al.* Sodium chloride inhibits the suppressive function of FOXP3+ regulatory T cells. *Journal of Clinical Investigation* **125**, 4212–4222 (2015).
10. Côrte-Real, B. F., Hamad I, Arroyo Hornero R, *et al.* Sodium perturbs mitochondrial respiration and induces dysfunctional Tregs. *Cell Metab* **35**, 299-315(2023).
11. Balan, Y., Packirisamy, R. M. & Mohanraj, P. S. High dietary salt intake activates inflammatory cascades via Th17 immune cells: impact on health and diseases. *Archives of Medical Science* **18**, 459–465 (2022).
12. Wilck, N., Matus MG, Kearney SM, *et al.* Salt-responsive gut commensal modulates TH17 axis and disease. *Nature* **551**, 585–589 (2017).
13. Kleinewietfeld, M., Manzel A, Titze J, *et al.* Sodium chloride drives autoimmune disease by the induction of pathogenic TH 17 cells. *Nature* **496**, 518–522 (2013).
14. Matthias, J., Heink S, Picard F, *et al.* Salt generates antiinflammatory Th17 cells but amplifies pathogenicity in proinflammatory cytokine microenvironments. *Journal of Clinical Investigation* **130**, 4587–4600 (2020).

15. Basile, D. P., Abais-Battad, J. M. & Mattson, D. L. Contribution of Th17 cells to tissue injury in hypertension. *Current Opinion in Nephrology and Hypertension* **30**, 151–158 (2021).
16. Wyatt, C. M. & Crowley, S. D. Intersection of salt- and immune-mediated mechanisms of hypertension in the gut microbiome. *Kidney Int* **93**, 532–534 (2018).
17. Wenzel UO, Ehmke H, Bode M., Immune mechanisms in arterial hypertension. *Journal of the American Society of Nephrology* **27**, 677–686 (2016).
18. Elijovich, F., Kleyman, T. R., Laffer, C. L. & Kirabo, A. Immune mechanisms of dietary salt-induced hypertension and kidney disease: Harry Goldblatt award for early career investigators 2020. Hypertension **78**, 252–260 (2021).
19. Weaver, C. T., Harrington, L. E., Mangan, P. R., Gavrieli, M. & Murphy, K. M. Th17: An Effector CD4 T Cell Lineage with Regulatory T Cell Ties. *Immunity* vol. 24 677–688 (2006).
20. Korn, T., Bettelli, E., Oukka, M. & Kuchroo, V. K. IL-17 and Th17 cells. *Annual Review of Immunology* vol. 27 485–517 (2009).
21. Muranski, P., Restifo, N. P. & Dc, W. Essentials of Th17 cell commitment and plasticity Review Article Essentials of Th17 cell commitment and plasticity.*Blood* **121**, 2402–2414 (2013).
22. Stockinger, B. Lumpers and splitters : Birth of Th17 cells. *J of Exp Med* **218**, 1–2 (2021).
23. Ohnmacht, C., Marques, R., Presley, L., Sawa, S., Lochner, M. and Eberl, G., *et al.* Intestinal microbiota, evolution of the immune system and the bad reputation of pro-inflammatory immunity. *Cellular Microbiology* vol. 13 653–659 (2011).
24. Orejudo, M., Rodrigues-Diez RR, Rodrigues-Diez R, *et al.* Interleukin 17A participates in renal inflammation associated to experimental and human hypertension. *Front Pharmacol* **10**, 1015 (2019).
25. Saleh, M. A., Norlander, A. E. & Madhur, M. S. Inhibition of Interleukin-17A, But Not Interleukin-17F, Signaling Lowers Blood Pressure, and Reduces End-Organ Inflammation in Angiotensin II-Induced Hypertension. *JACC Basic Transl Sci.* **7***, 606-616.* (2016).
26. Nguyen, H. Chiasson VL, Chatterjee P, Kopriva SE, Young KJ, Mitchell BM. Interleukin-17 causes Rho-kinase-mediated endothelial dysfunction and hypertension. *Cardiovasc Res* **97**, 696–704 (2013).
27. Aguiar, S. L. F., Miranda M.C.G., Guimarães M.A.F., *et al.* High-salt diet induces IL-17-dependent gut inflammation and exacerbates colitis in mice. *Front Immunol* **8**, (2018).
28. Madhur, MS, Lob HE, McCann LA, Iwakura Y, Blinder Y, Guzik TJ, Harrison DG. *et al.* Interleukin 17 promotes angiotensin II-induced hypertension and vascular dysfunction. *Hypertension* **55,** 500–507 (2010)
29. Lee, PW, Smith AJ, Yang Y, *et al.* IL-23R–activated STAT3/STAT4 is essential for Th1/Th17-mediated CNS autoimmunity. *JCI Insight* **2**, e91663 (2017).
30. Wu, C., Yosef, N., Thalhamer, T. *et al.* Induction of pathogenic TH 17 cells by inducible salt-sensing kinase SGK1. *Nature* **496**, 513–517 (2013).
31. Bettelli, E., Carrier, Y., Gao, W. *et al.* Reciprocal developmental pathways for the generation of pathogenic effector TH17 and regulatory T cells. *Nature* **441**, 235–238 (2006).
32. Veldhoen, M., Hocking, R. J., Atkins, C. J., Locksley, R. M. & Stockinger, B. TGFβ in the context of an inflammatory cytokine milieu supports de novo differentiation of IL-17-producing T cells. *Immunity* **24**, 179–189 (2006).
33. Omenetti, S. Bussi C, Metidji A, *et al.* The Intestine Harbors Functionally Distinct Homeostatic Tissue-Resident and Inflammatory Th17 Cells. *Immunity* **51**, 77-89 (2019).

34. Lin YH, Duong HG, Limary AE, *et al.* Small intestine and colon tissue-resident memory CD8+ T cells exhibit molecular heterogeneity and differential dependence on Eomes. *Immunity* **56**, 207-223 (2023).
35. Konjar Š, Ferreira C, Carvalho FS, Figueiredo-Campos P, Fanczal J, Ribeiro S, Morais VA, Veldhoen M. Intestinal tissue-resident T cell activation depends on metabolite availability. *Proc Natl Acad Sci U S A.* **119,** e2202144119 (2022).
36. Kuo, S., El Guindy, A., Panwala, C. M., Hagan, P. M. & Camerini, V. Differential Appearance of T Cell Subsets in the Large and Small Intestine of Neonatal Mice. *Pediatric Research* **49**, 543-51 (2001).
37. Amamou, A., Rouland, M., Yaker, L. *et al.* Dietary salt exacerbates intestinal fibrosis in chronic TNBS colitis via fibroblasts activation. *Sci Rep* **11**, 15055 (2021).
38. Miranda PM, De Palma G, Serkis V, *et al.* High salt diet exacerbates colitis in mice by decreasing Lactobacillus levels and butyrate production. *Microbiome* **6**, 57 (2018).
39. Allison, S. J. Autoimmune disease: Egress of intestinal T H 17 cells in autoimmune renal disease. *Nature Reviews Nephrology* **13**, 61 (2017).
40. Krebs CF, Turner JE, Paust HJ, *et al.* Plasticity of Th17 Cells in Autoimmune Kidney Diseases. *The Journal of Immunology* **197**, 449–457 (2016).
41. Jain R, Chen Y, Kanno Y, *et al.* Interleukin-23-Induced Transcription Factor Blimp-1 Promotes Pathogenicity of T Helper 17 Cells. *Immunity* **44**, 131–142 (2016).
42. Ghoreschi, K., Laurence, A., Yang, XP. *et al*. Generation of pathogenic TH 17 cells in the absence of TGF-β 2 signalling. *Nature* **467**, 967–971 (2010).
43. Schnell A, Littman DR, Kuchroo VK. TH17 cell heterogeneity and its role in tissue inflammation. *Nature Immunology* **24**, 19–29 (2023).
44. Schnell A, Huang L, Singer M, *et al.* Stem-like intestinal Th17 cells give rise to pathogenic effector T cells during autoimmunity. *Cell* **184**, 6281-6298 (2021).
45. Rucker AJ, Rudemiller NP, Crowley SD, *et al*. Salt, Hypertension, and Immunity. *Annu Rev Physiol* **80**, 283–307 (2018)
46. Haase, S., Wilck N., Kleinewietfeld M., Muller D.N, Linker, R., Sodium chloride triggers Th17 mediated autoimmunity. *Journal of Neuroimmunology* **329**, 9–13 (2019)
47. Avery, E. G., Bartolomaeus H., Rauch A., *et al.* Quantifying the impact of gut microbiota on inflammation and hypertensive organ damage. *Cardiovasc Res* **119**, 1441–1452 (2023).
48. Zelante, T, Iannitti RG, Cunha C, *et al*. Tryptophan catabolites from microbiota engage aryl hydrocarbon receptor and balance mucosal reactivity via interleukin-22. *Immunity* **39**, 372–385 (2013).
49. Kimura, A., Naka, T., Nohara, K., Fujii-Kuriyama, Y. & Kishimoto, T. Aryl Hydrocarbon Receptor Regulates Stat1 Activation and Participates in the Development of Th17 Cells. *Proc Natl Acad Sci U S A*. **105**, 9721-9726. (2008).
50. de Lima, K.A., Donate, P.B., Talbot, J. *et al.* TGFβ1 signaling sustains aryl hydrocarbon receptor (AHR) expression and restrains the pathogenic potential of TH17 cells by an AHR-independent mechanism. *Cell Death Dis* **9**, 1130, (2018).
51. Duarte, J. H., Di Meglio, P., Hirota, K., Ahlfors, H. & Stockinger, B. Differential influences of the aryl hydrocarbon receptor on Th17 mediated responses in vitro and in vivo. *PLoS One* **8**, e79819 (2013).

52. Graelmann FJ, Gondorf F, Majlesain Y, *et al.* Differential cell type-specific function of the aryl hydrocarbon receptor and its repressor in diet-induced obesity and fibrosis. *Mol Metab* **85,** 101963 (2024).
53. Zhang Q, Zhu Y, Lv C, *et al.* AhR activation promotes Treg cell generation by enhancing Lkb1-mediated fatty acid oxidation via the Skp2/K63-ubiquitination pathway. *Immunology* **169**, 412–430 (2023).
54. Dean JW, Helm EY, Fu Z, *et al.* The aryl hydrocarbon receptor cell intrinsically promotes resident memory CD8+ T cell differentiation and function. *Cell Rep* **42,** 111963 (2023).
55. Quintana FJ, Basso AS, Iglesias AH, *et al.* Control of Treg and TH17 cell differentiation by the aryl hydrocarbon receptor. *Nature* **453**, 65–71 (2008).
56. Schanz O, Chijiiwa R, Cengiz SC, *et al.* Dietary aHR ligands regulate ahrr expression in intestinal immune cells and intestinal microbiota composition. *Int J Mol Sci* **21**, 3189 (2020).
57. Agus, A., Planchais, J. & Sokol, H. Gut Microbiota Regulation of Tryptophan Metabolism in Health and Disease. *Cell Host Microbe* **23**, 716–724 (2018).
58. McCarville, J. L., Chen, G. Y., Cuevas, V. D., Troha, K. & Ayres, J. S. Microbiota Metabolites in Health and Disease. *Annu Rev Immunol* **38**, 147–170 (2020).
59. Goettel JA, Gandhi R, Kenison JE, *et al.* AHR Activation Is Protective against Colitis Driven by T Cells in Humanized Mice. *Cell Rep* **17**, 1318–1329 (2016).
60. Ivanov II, Atarashi K, Manel N, *et al.* Induction of Intestinal Th17 Cells by Segmented Filamentous Bacteria. *Cell* **139**, 485–498 (2009).
61. Woo V, Eshleman EM, Hashimoto-Hill S, *et al.* Commensal segmented filamentous bacteria-derived retinoic acid primes host defense to intestinal infection. *Cell Host Microbe* **29**, 1744-1756 (2021).
62. Goto Y, Panea C, Nakato G, *et al.* Segmented filamentous bacteria antigens presented by intestinal dendritic cells drive mucosal Th17 cell differentiation. *Immunity* **40**, 594–607 (2014).
63. Lécuyer E, Rakotobe S, Lengliné-Garnier H, *et al.* Segmented filamentous bacterium uses secondary and tertiary lymphoid tissues to induce gut IgA and specific T helper 17 cell responses. *Immunity* **40**, 608–620 (2014).
64. Al Nabhani Z, Dulauroy S, Marques R, *et al.* A Weaning Reaction to Microbiota Is Required for Resistance to Immunopathologies in the Adult. *Immunity* **50**, 1276-1288 (2019).
65. Caruso, R., Ono, M., Bunker, M. E., Núñez, G. & Inohara, N. Dynamic and Asymmetric Changes of the Microbial Communities after Cohousing in Laboratory Mice. *Cell Rep* **27**, 3401-3412 (2019).
66. Nowotschin, S. & Hadjantonakis, A. K. Use of KikGR a photoconvertible green-to-red fluorescent protein for cell labeling and lineage analysis in ES cells and mouse embryos. *BMC Dev Biol* **9**, 49 (2009).
67. Van Beusecum JP, Barbaro NR, McDowell Z, *et al.* High Salt Activates CD11c+ Antigen-Presenting Cells via SGK (Serum Glucocorticoid Kinase) 1 to Promote Renal Inflammation and Salt-Sensitive Hypertension. *Hypertension* **74**, 555–563 (2019).
68. Itani HA, Xiao L, Saleh MA, *et al.* CD70 exacerbates blood pressure elevation and renal damage in response to repeated hypertensive stimuli. *Circ Res* **118**, 1233–1243 (2016).
69. Busbee PB, Menzel L, Alrafas HR, *et al.* Indole-3-carbinol prevents colitis and associated microbial dysbiosis in an IL-22–dependent manner. *JCI Insight* **5**, e127551(2020).

70. Anderton MJ, Manson MM, Verschoyle RD, *et al.* Pharmacokinetics and tissue disposition of indole-3-carbinol and its acid condensation products after oral administration to mice. *Clinical Cancer Research* **10**, 5233–5241 (2004).
71. Obata Y, Castaño Á, Boeing S, *et al.* Neuronal programming by microbiota regulates intestinal physiology. *Nature* **578**, 284–289 (2020).
72. Tomura M, Yoshida N, Tanaka J, *et al.* Monitoring cellular movement in vivo with photoconvertible fluorescence protein 'Kaede' transgenic mice. *Proc Nat Acad Sci USA* **105**, 10871–10876 (2008).
73. Galván-Peña, S., Zhu, Y., Hanna, B. S., Mathis, D. & Benoist, C. A dynamic atlas of immunocyte migration from the gut. *Sci Immunol* **9**, 0672 (2024).
74. Nagai M, Noguchi R, Takahashi D, *et al.* Fasting-Refeeding Impacts Immune Cell Dynamics and Mucosal Immune Responses. *Cell* **178**, 1072-1087 (2019).
75. Benakis C, Brea D, Caballero S, *et al.* Commensal microbiota affects ischemic stroke outcome by regulating intestinal γδ T cells. *Nat Med* **22**, 516–523 (2016).
76. Nakanishi Y, Ikebuchi R, Chtanova T, *et al.* Regulatory T cells with superior immunosuppressive capacity emigrate from the inflamed colon to draining lymph nodes. *Mucosal Immunol* **11**, 437–448 (2018).
77. Harrington LE, Hatton RD, Mangan PR, *et al.* Interleukin 17-producing CD4+ effector T cells develop via a lineage distinct from the T helper type 1 and 2 lineages. *Nat Immunol* **6**, 1123–1132 (2005).
78. Harbour, S. N., Maynard, C. L., Zindl, C. L., Schoeb, T. R. & Weaver, C. T. Th17 cells give rise to Th1 cells that are required for the pathogenesis of colitis. *Proc Natl Acad Sci U S A* **112**, 7061–7066 (2015).
79. Withers DR, Hepworth MR, Wang X, *et al.* Transient inhibition of ROR-γt therapeutically limits intestinal inflammation by reducing TH17 cells and preserving group 3 innate lymphoid cells. *Nat Med* **22**, 319–323 (2016).
80. Hepworth MR, Fung TC, Masur SH, *et al.* Group 3 Innate Lymphoid Cells Mediate Intestinal Selection of Commensal Bacteria-Specific CD4 + T Cells. *Science* **348**, 1031-1035 (2015).
81. Maynard CL, Harrington LE, Janowski KM, *et al.* Regulatory T cells expressing interleukin 10 develop from Foxp3+ and Foxp3- precursor cells in the absence of interleukin 10. *Nat Immunol* **8**, 931–941 (2007).
82. Withers DR, Hepworth MR, Wang X, *et al.* Transient inhibition of ROR-γt therapeutically limits intestinal inflammation by reducing TH17 cells and preserving group 3 innate lymphoid cells. *Nat Med* **22**, 319–323 (2016).
83. Futamura K, Sekino M, Hata A, *et al.* Novel full-spectral flow cytometry with multiple spectrally-adjacent fluorescent proteins and fluorochromes and visualization of in vivo cellular movement. *Cytometry Part A* **87**, 830–842 (2015).
84. Yosef N, Shalek AK, Gaublomme JT, *et al.* Dynamic regulatory network controlling TH 17 cell differentiation. *Nature* **496**, 461–468 (2013).
85. Lee JY, Hall JA, Kroehling L,*et al.* Serum Amyloid A Proteins Induce Pathogenic Th17 Cells and Promote Inflammatory Disease. *Cell* **180**, 79-91 (2020).
86. Speed JS, Hyndman KA, Kasztan M, *et al.* Diurnal pattern in skin Na and water content is associated with salt-sensitive hypertension in ETB receptor-deficient rats. *Am J Physiol Regul Integr Comp Physiol* **314**, 544–551 (2018).

87. Ouyang, W. & O'Garra, A. IL-10 Family Cytokines IL-10 and IL-22: from Basic Science to Clinical Translation. *Immunity* **50**, 871–891 (2019).
88. Eyerich, K., Dimartino, V. & Cavani, A. IL-17 and IL-22 in immunity: Driving protection and pathology. *Eur J Immunol* **47**, 607–614 (2017).
89. Basu R, O'Quinn DB, Silberger DJ, *et al.* Th22 Cells Are an Important Source of IL-22 for Host Protection against Enteropathogenic Bacteria. *Immunity* **37**, 1061–1075 (2012).
90. Cardilli A, Hamad I, Dyczko A, *et al.* Impact of High Salt-Intake on a Natural Gut Ecosystem in Wildling Mice. *Nutrients* **15**, 1565 (2023).
91. Thowsen IM, Reikvam T, Skogstrand T, *et al.* Genetic Engineering of Lymphangiogenesis in Skin Does Not Affect Blood Pressure in Mouse Models of Salt-Sensitive Hypertension. *Hypertension* **79**, 2451–2462 (2022).
92. Brockmann L, Tran A, Huang Y, *et al.* Intestinal microbiota-specific Th17 cells possess regulatory properties and suppress effector T cells via c-MAF and IL-10. *Immunity* **56**, 2719-2735 (2023).
93. Cao, A. T., Yao, S., Gong, B., Elson, C. O. & Cong, Y. Th17 Cells Upregulate Polymeric Ig Receptor and Intestinal IgA and Contribute to Intestinal Homeostasis. *Journal of Immunology* **189**, 4666–4673 (2012).
94. Nakamura T, Kurihara I, Kobayashi S, *et al.* Intestinal mineralocorticoid receptor contributes to epithelial sodium channel–mediated intestinal sodium absorption and blood pressure regulation. *J Am Heart Assoc* **7**, e008259 (2018).
95. Suckling, R. J., He, F. J., Markandu, N. D. & MacGregor, G. A. Dietary salt influences postprandial plasma sodium concentration and systolic blood pressure. *Kidney Int* **81**, 407–411 (2012).
96. Hyndman KA, Mironova EV, Giani JF, *et al.* Collecting duct nitric oxide synthase 1ß activation maintains sodium homeostasis during high sodium intake through suppression of aldosterone and renal angiotensin II pathways. *J Am Heart Assoc* **6**, e006896 (2017).
97. Gohar EY, De Miguel C, Obi IE, *et al.* Acclimation to a High-Salt Diet Is Sex Dependent. *J Am Heart Assoc* **11**, e020450 (2022).
98. Speed JS, Hyndman KA, Roth K,*et al.* High dietary sodium causes dyssynchrony of the renal molecular clock in rats. *Am J Physiol Renal Physiol* **314**, 89–98 (2018).
99. Ivanov II, McKenzie BS, Zhou L, *et al.* The Orphan Nuclear Receptor RORγt Directs the Differentiation Program of Proinflammatory IL-17+ T Helper Cells. *Cell* **126**, 1121–1133 (2006).
100. Prados A, Onder L, Cheng HW, *et al.* Fibroblastic reticular cell lineage convergence in Peyer's patches governs intestinal immunity. *Nat Immunol* **22**, 510–519 (2021).
101. Chang, J. E., Buechler, M. B., Gressier, E., Turley, S. J. & Carroll, M. C. Mechanosensing by Peyer's patch stroma regulates lymphocyte migration and mucosal antibody responses. *Nat Immunol* **20**, 1506–1516 (2019).
102. Hirota K, Turner JE, Villa M, *et al.* Plasticity of TH 17 cells in Peyer's patches is responsible for the induction of T cell-dependent IgA responses. *Nat Immunol* **14**, 372–379 (2013).
103. Hirota K, Duarte JH, Veldhoen M, *et al.* Fate mapping of IL-17-producing T cells in inflammatory responses. *Nat Immunol* **12**, 255–263 (2011).
104. Zhao, Q. & Maynard, C. L. Mucus, commensals, and the immune system. *Gut Microbes* **14,** 2041342 (2022).
105. Siracusa, F., Schaltenberg, N., Kumar, Y. *et al*. Short-term dietary changes can result in mucosal and systemic immune depression. *Nat Immunol* **24**, 1473–1486 (2023).

106. Al Nabhani Z, Dulauroy S, Lécuyer E,. *et al.* Excess calorie intake early in life increases susceptibility to colitis in adulthood. *Nat Metab* **1**, 1101–1109 (2019).
107. Garidou L, Pomié C, Klopp P, *et al.* The Gut Microbiota Regulates Intestinal CD4 T Cells Expressing RORγt and Controls Metabolic Disease. *Cell Metab* **22**, 100–112 (2015).
108. Joshi P, McCann GJP, Sonawane VR, Vishwakarma RA, Chaudhuri B, Bharate SB. Identification of Potent and Selective CYP1A1 Inhibitors via Combined Ligand and Structure-Based Virtual Screening and Their in Vitro Validation in Sacchrosomes and Live Human Cells. *J Chem Inf Model* **57**, 1309–1320 (2017).
109. Groom, J. R. Regulators of T-cell fate: Integration of cell migration, differentiation and function. *Immunological Reviews* **289**, 101–114 (2019).
110. Duckworth BC, Lafouresse F, Wimmer VC, *et al.* Effector and stem-like memory cell fates are imprinted in distinct lymph node niches directed by CXCR3 ligands. *Nat Immunol* **22**, 434–448 (2021).
111. Veldhoen, M. & Ferreira, C. Influence of nutrient-derived metabolites on lymphocyte immunity. *Nat Med* **21**, 709–718 (2015).
112. Veldhoen, M., Hirota, K., Christensen, J., O'Garra, A. & Stockinger, B. Natural agonists for aryl hydrocarbon receptor in culture medium are essential for optimal differentiation of Th17 T cells. *Journal of Experimental Medicine* **206**, 43–49 (2009).
113. Smirnova A, Wincent E, Vikström Bergander L, *et al.* Evidence for New Light-Independent Pathways for Generation of the Endogenous Aryl Hydrocarbon Receptor Agonist FICZ. *Chem Res Toxicol* **29**, 75–86 (2016).
114. Rannug, A. How the AHR became important in intestinal homeostasis—A diurnal FICZ/AHR/CYP1A1 feedback controls both immunity and immunopathology. *Int J Mol Sci* **21**, 1–19 (2020).
115. Vyhlídalová B, Krasulová K, Pečinková P, *et al.* Gut microbial catabolites of tryptophan are ligands and agonists of the aryl hydrocarbon receptor: A detailed characterization. *Int J Mol Sci* **21**, 1–17 (2020).
116. Gutiérrez-Vázquez, C. & Quintana, F. J. Regulation of the Immune Response by the Aryl Hydrocarbon Receptor. *Immunity* **48**, 19–33 (2018).
117. Ranasinghe, R. & Eri, R. CCR6–CCL20-Mediated Immunologic Pathways in Inflammatory Bowel Disease. *Gastrointestinal Disorders* **1**, 15–29 (2018).
118. Wang, C., Kang, S. G., Lee, J., Sun, Z. & Kim, C. H. The roles of CCR6 in migration of Th17 cells and regulation of effector T-cell balance in the gut. *Mucosal Immunol* **2**, 173–183 (2009).
119. Santisteban MM, Qi Y, Zubcevic J, *et al.* Hypertension-Linked Pathophysiological Alterations in the Gut. *Circ Res* **120**, 312–323 (2017).
120. Zhao Q, Harbour SN, Kolde R, *et al.* Selective Induction of Homeostatic Th17 Cells in the Murine Intestine by Cholera Toxin Interacting with the Microbiota. *The Journal of Immunology* **199**, 312–322 (2017).
121. Lee JS, Tato CM, Joyce-Shaikh B, *et al.* Interleukin-23-Independent IL-17 Production Regulates Intestinal Epithelial Permeability. *Immunity* **43**, 727–738 (2015).
122. Krausgruber T, Schiering C, Adelmann K, *et al.* T-bet is a key modulator of IL-23-driven pathogenic CD4+ T cell responses in the intestine. *Nat Commun* **7**, 11627 (2016).
123. Crowley, S. D. & Jeffs, A. D. Targeting cytokine signaling in salt-sensitive hypertension. *Am J Physiol Renal Physiol* **311**, 1153–1158 (2016).

124. Zhang MZ, Yao B, Wang Y, Yang S, Wang S, Fan X, Harris RC. Inhibition of cyclooxygenase-2 in hematopoietic cells results in salt-sensitive hypertension. *Journal of Clinical Investigation* **125**, 4281–4294 (2015).
125. Santisteban MM, Schaeffer S, Anfray A*, et al.* Meningeal interleukin-17-producing T cells mediate cognitive impairment in a mouse model of salt-sensitive hypertension. *Nat Neurosci* **27**, 63–77 (2024).
126. He W, Xu J, Mu R, *et al.* High-salt diet inhibits tumour growth in mice via regulating myeloid-derived suppressor cell differentiation. *Nat Commun* **11**, 1732 (2020).
127. Robertson SJ, Lemire P, Maughan H, *et al.* Comparison of Co-housing and Littermate Methods for Microbiota Standardization in Mouse Models. *Cell Rep* **27**, 1910-1919 (2019).
128. Ji H, Pai AV, West CA, Wu X, Speth RC, Sandberg K. Loss of Resistance to Angiotensin II-Induced Hypertension in the Jackson Laboratory Recombination-Activating Gene Null Mouse on the C57BL/6J Background. *Hypertension* **69**, 1121–1127 (2017).
129. Savignac, H. M., Dinan, T. G. & Cryan, J. F. Resistance to Early-Life Stress in Mice: Effects of Genetic Background and Stress Duration. *Front Behav Neurosci* **5**, 1–12 (2011).
130. Pugh, P. L., Ahmed, S. F., Smith, M. I., Upton, N. & Hunter, A. J. A behavioural characterisation of the FVB/N mouse strain. *Behavioural Brain Research* **155**, 283–289 (2004).
131. Morgan JL, Svenson KL, Lake JP, *et al.* Effects of housing density in five inbred strains of mice. *PLoS One* **9**, e90012 (2014).
132. Zhu L, Wu Z, Zhu C, Yin J, Huang Y, Feng J, Zhang Q. The Deletion of IL-17A Enhances Helicobacter hepaticus Colonization and Triggers Colitis. *J Inflamm Res* **15**, 2761–2773 (2022).
133. Campisi L, Barbet G, Ding Y, Esplugues E, Flavell RA, Blander JM. Apoptosis in response to microbial infection induces autoreactive T H17 cells. *Nat Immunol* **17**, 1084–1092 (2016).
134. Ghoreschi K, Laurence A, Yang XP, *et al* Generation of pathogenic TH 17 cells in the absence of TGF-β 2 signalling. *Nature* **467**, 967–971 (2010).
135. Krebs CF, Paust HJ, Krohn S, *et al.* Autoimmune Renal Disease Is Exacerbated by S1P-Receptor-1-Dependent Intestinal Th17 Cell Migration to the Kidney. *Immunity* **45**, 1078–1092 (2016).
136. Granados JC, Falah K, Koo I, *et al.* AHR is a master regulator of diverse pathways in endogenous metabolism. *Sci Rep* **12**, 16625 (2022).
137. Manzella C, Singhal M, Alrefai WA, Saksena S, Dudeja PK, Gill RK. Serotonin is an endogenous regulator of intestinal CYP1A1 via AhR. *Sci Rep* **8**, 6103 (2018).
138. Krebs CF, Lange S, Niemann G, *et al.* Deficiency of the Interleukin 17/23 Axis Accelerates Renal Injury in Mice With Deoxycorticosterone Acetate+Angiotensin II-Induced Hypertension Kidney. *Hypertension* **63,** 565-71 (2013).
139. Navar LG, Mitchell KD, Harrison-Bernard LM, Kobori H, Nishiyama A. Review: Intrarenal angiotensin II levels in normal and hypertensive states. *Journal of the Renin-Angiotensin-Aldosterone System* **2,** S176-S184 (2001).
140. Markó L, Kvakan H, Park JK, *et al.* Interferon-γ Signaling Inhibition Ameliorates Angiotensin II-Induced Cardiac Damage Heart. Hypertension. **60**, 1430-6. (2012).
141. Li B, He X, Lei SS, *et al.* Hypertensive rats treated chronically with Nω-Nitro-L-Arginine Methyl Ester (L-NAME) induced disorder of hepatic fatty acid metabolism and intestinal pathophysiology. *Front Pharmacol* **10**, 1677 (2020).

142. Kahalehili HM, Newman NK, Pennington JM, *et al.* Dietary Indole-3-Carbinol Activates AhR in the Gut, Alters Th17-Microbe Interactions, and Exacerbates Insulitis in NOD Mice. *Front Immunol* **11**, 606441 (2021).
143. Yue, T. *et al.* The AHR Signaling Attenuates Autoimmune Responses During the Development of Type 1 Diabetes. *Frontiers in Immunology* **11**, 1510 (2020).
144. Liu, W. C., Chen, P. H. & Chen, L. W. Supplementation of endogenous Ahr ligands reverses insulin resistance and associated inflammation in an insulin-dependent diabetic mouse model. *Journal of Nutritional Biochemistry* **83**, 108384 (2020).
145. Xiong L, Dean JW, Fu Z, *et al.* Ahr-Foxp3-RORγt axis controls gut homing of CD4+ T cells by regulating GPR15. *Sci Immunol* **5**, 1–15 (2020).
146. Stockinger, B., Shah, K. & Wincent, E. AHR in the intestinal microenvironment: safeguarding barrier function. *Nature Reviews Gastroenterology and Hepatology* **18**, 559–570 (2021).
147. Diny NL, Schonfeldova B, Shapiro M, Winder ML, Varsani-Brown S, Stockinger B.. The aryl hydrocarbon receptor contributes to tissue adaptation of intestinal eosinophils in mice. *Journal of Experimental Medicine* **219**, e20210970 (2022).
148. Metidji A, Omenetti S, Crotta S, *et al.* The Environmental Sensor AHR Protects from Inflammatory Damage by Maintaining Intestinal Stem Cell Homeostasis and Barrier Integrity. *Immunity* **49**, 353-362 (2018).
149. Chen J, Haller CA, Jernigan FE, *et al.* Modulation of lymphocyte-mediated tissue repair by rational design of heterocyclic aryl hydrocarbon receptor agonists. *Sci Adv* **6**, 1–16 (2020).

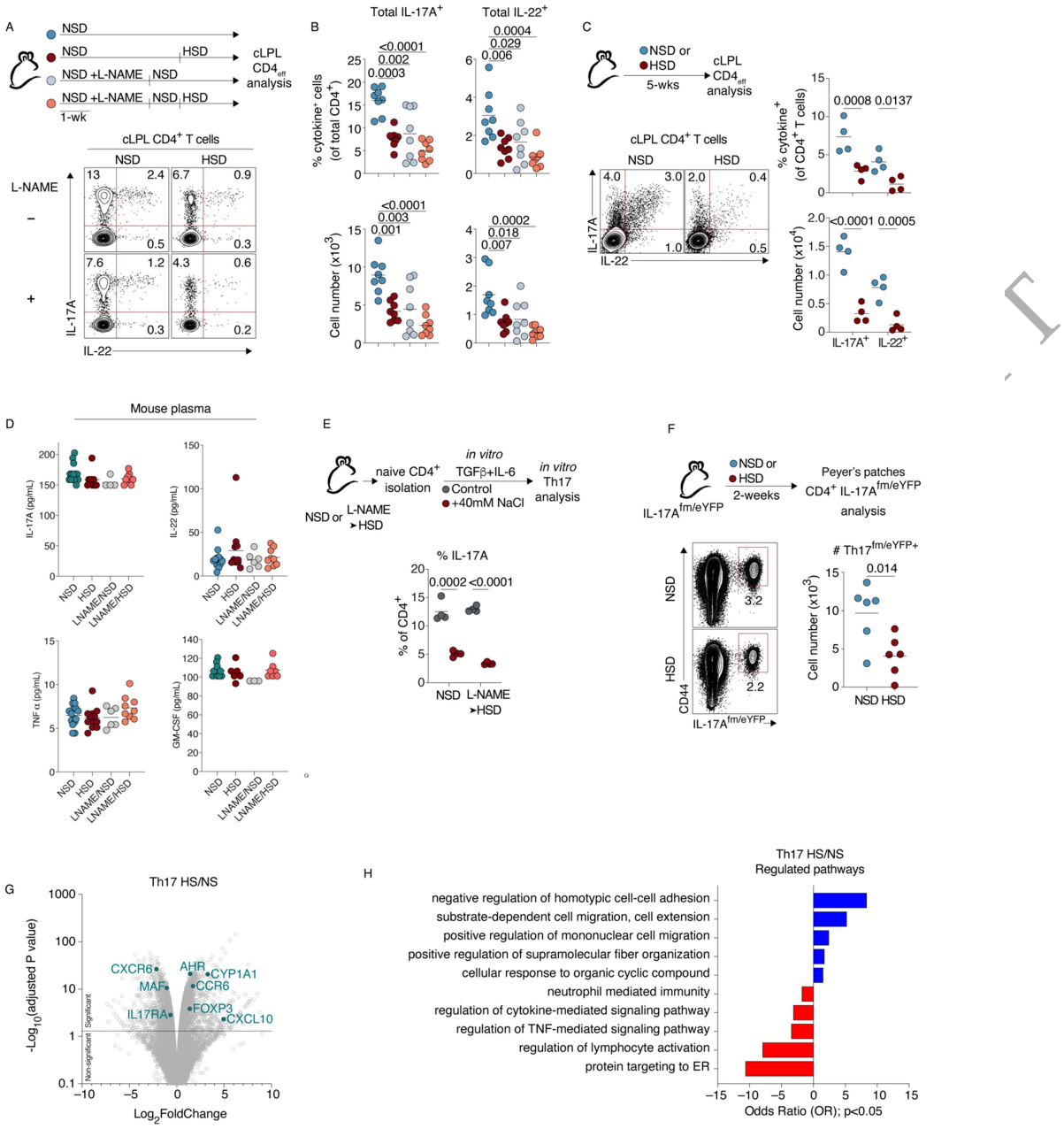

Figure 1. HSD, independent of hypertension, depresses CD4$^+$ T cell cytokine expression

Figure 1. HSD, independent of hypertension, depresses CD4$^+$ T cell cytokine expression. A) Experimental schematic outlining salt-sensitive model with representative FACS plots identifying

IL-17A and IL-22 produced by $CD4^+$ T cells. Numbers within quadrants indicate frequency among $CD4^+$ T cells. B) IL-17A and IL-22 cytokine frequencies among $CD4^+$ T cells and absolute numbers. C) Experimental scheme outlining 5-weeks of HSD feeding, analysis of IL-17A and IL-22-expressing effector T cells among cLPLs in mice fed 5-weeks NSD or HSD. D) Circulating cytokine concentrations from NSD-fed mice, HSD-fed mice, NSD-fed salt sensitive mice, and HSD-fed salt-sensitive mice. E) Experimental schematic outlining naïve $CD4^+$ T cell sorting from mice fed a NSD or salt-sensitive mice fed HSD followed by Th17 *in vitro* polarization and frequency among polarized $CD4^+$ T cells. Polarizing cells were re-stimulated with PMA/Ionomycin followed by cytokine sequestration with brefeldin. F) Experimental schematic to evaluate the effect of *in vivo* HSD feeding on Peyer's patches Th17 cells, representative FACS plots of $CD4^+$ T cells showing staining for CD44 and fm/eYFP signal, and absolute cell count. G) Volcano plot with mean $\log_2$-transformed fold change (x-axis) and significance ($-\log_{10}$(adjusted P-value)) of differentially expressed genes (DEGs, DESeq2 analysis) among isolated human $CD4^+$ T cells polarized under Th17 conditions in the presence of high salt vs normal salt media (data downloaded from Gene Expression Omnibus, GSE148669[6]). H) Gene ontology biological process pathway enrichment analysis with ClusterProfiler showing significantly enriched gene sets among isolated human $CD4^+$ T cells polarized under Th17 conditions in the presence of high salt vs normal salt media (data downloaded from Gene Expression Omnibus, GSE148669[6]). ns, not significant ($p>0.05$); $*p\leq0.05$; $**p\leq0.01$; $***p\leq0.001$; $****p\leq0.0001$; Two-way ANOVA (B, C, E) and student's two-tailed t test (D and F). Volcano plot of RNA analysis with $\log_2$-transformed fold change and ($-\log_{10}$(adjusted P-value)) (G), and gene ontology analysis among human Th17 cells treated with HS-to-NS (H).

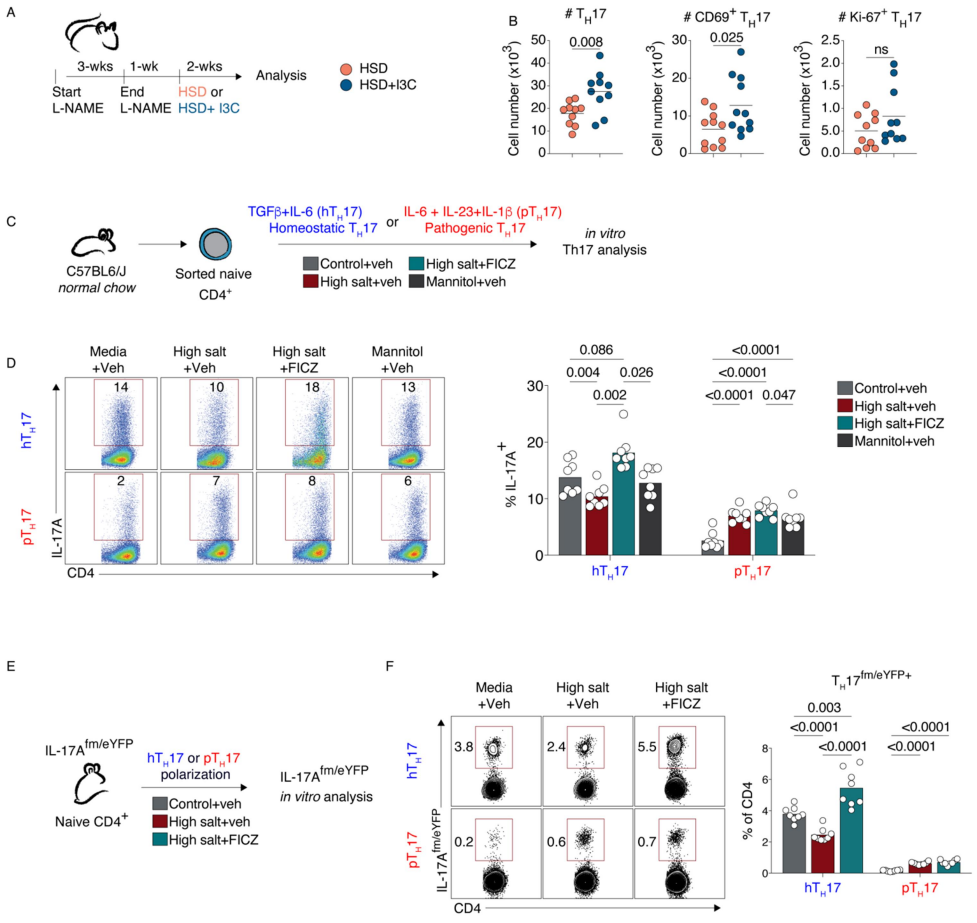

Figure 2. AhR activation promotes Th17 expansion during excess salt intake and exposure

Figure 2. AhR activation promotes Th17 expansion during excess salt intake and exposure. A) Experimental schematic for Th17 analysis in HSD-fed and HSD+I3C (indole-3-

carbinol) fed mice. B) Absolute cell numbers among Peyer's patch $CD4^+$ T cells from salt-sensitive mice fed a HSD or HSD with I3C for two weeks. C) Experimental scheme for naive $CD4^+$ *in vitro* polarizations evaluating Th17 differentiation under vehicle (DMSO), high salt + vehicle, high salt with FICZ (AhR activator), or mannitol. D) Representative FACS plots with respective frequency data for Th17 differentiation under homeostatic and pathogenic conditions for cells treated under vehicle (DMSO), high salt + vehicle, high salt + FICZ, or mannitol + vehicle. Polarizing cells were re-stimulated with PMA/Ionomycin followed by cytokine sequestration with brefeldin. E) Experimental schematic evaluating *in vitro* IL-$17A^{fm/eYFP}$ expression during Th17 differentiation with vehicle (DMSO), high salt+vehicle, or high salt with FICZ (AhR activator) under homeostatic and pathogenic polarizing conditions. Polarizing cells were re-stimulated with PMA/Ionomycin followed by cytokine sequestration with brefeldin. ns, not significant ($p>0.05$); $*p\leq0.05$; $**p\leq0.01$; $***p\leq0.001$; $****p\leq0.0001$; Student's two-tailed t test (B) and two-way ANOVA (D and F).

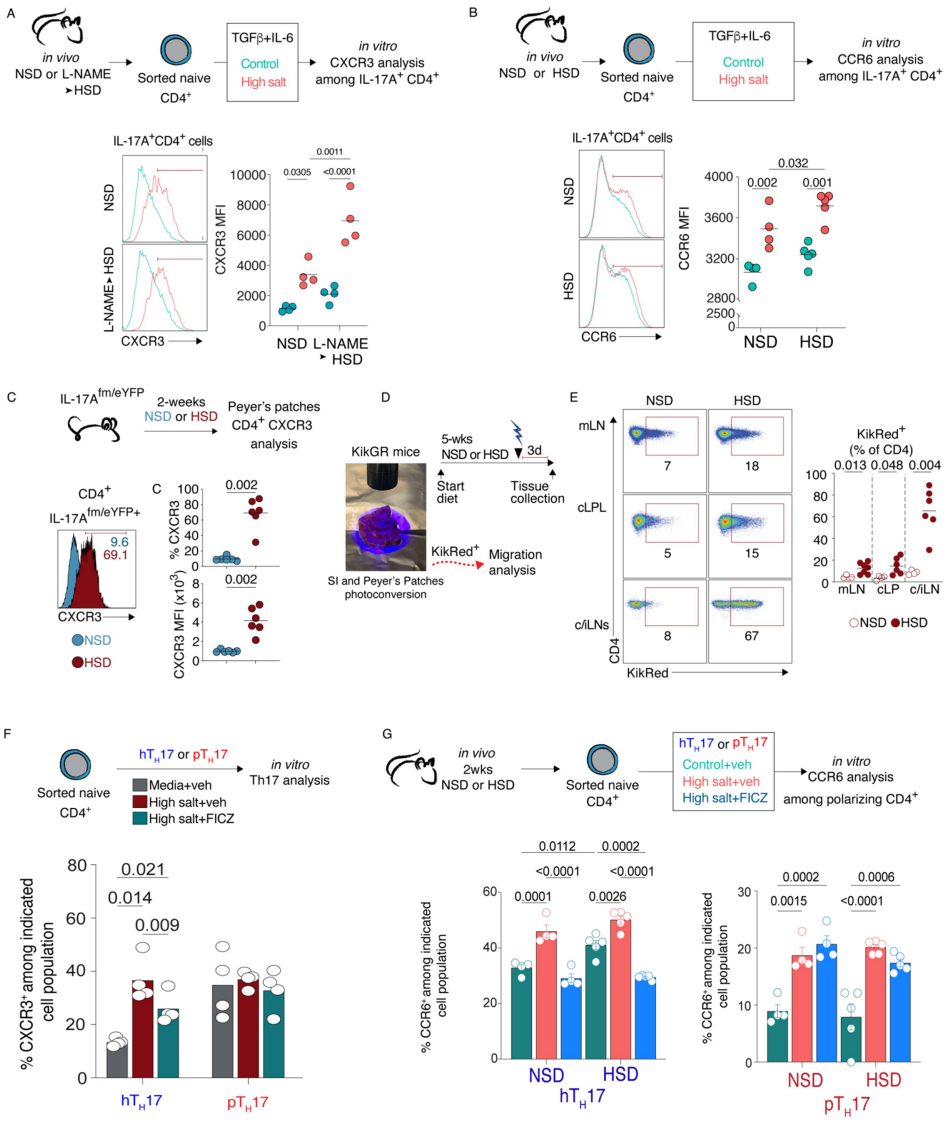

Figure 3. Activating AhR regulates features of mobilization induced by HSD in CD4+ T cells

Figure 3. Activating AhR regulates features of mobilization induced by HSD in CD4+ T cells. A) Experimental scheme for naïve CD4+ T cells isolated from NSD-fed or HSD-fed salt-sensitive mice followed by polarization under TGFβ + IL-6 differentiation conditions. CXCR3 median

fluorescence intensity (MFI) analysis on polarizing IL-17A$^+$ CD4$^+$ T cells with and without additional 40mM NaCl from NSD-fed and HSD-fed salt-sensitive mice. B) Experimental scheme for naïve CD4$^+$ T cells isolated from NSD-fed or HSD-fed mice followed by polarization under TGF$\boldsymbol{\beta}$ + IL-6 differentiation conditions. CCR6 MFI analysis on polarizing IL-17A$^+$ CD4$^+$ T cells with and without additional 40mM NaCl from NSD-fed and HSD-fed salt-sensitive mice. C) Experimental scheme for analysis of CXCR3 frequency and MFI among Th17 fate cells from the Peyer's patches of NSD-fed or HSD-fed mice. D) Diagram for experimental approach to photoconvert intestinal tissue from KikGR mice using a 405nm light and experimental scheme for KikRed$^+$CD4$^+$ T cells frequency among the mesenteric lymph nodes (mLN), colonic lamina propria lymphocytes (cLPL), and pooled caudal/iliac lymph nodes (c/iLN) from KikGR mice fed either a NSD or HSD. E) Representative gating and analysis of KikRed$^+$CD4$^+$ T cell frequency among mLN, cLPL, and c/iLNs from KikGR mice fed a NSD or HSD. F) Experimental scheme for polarization of wild-type naïve CD4+ T cells polarized under homeostatic or pathogenic Th17 conditions treated with vehicle (DMSO), high salt + vehicle, or high salt with FICZ (AhR activator). CXCR3 frequency among IL-17A$^+$ CD4$^+$ T cells was analyzed to determine regulation of CXCR3 expression in response to high salt or high salt + AhR activator (FICZ) under homeostatic or pathogenic Th17 conditions. G) Experimental scheme for polarization of wildtype naïve CD4$^+$ T cells from mice fed 2-weeks of NSD or HSD followed by homeostatic (TGFβ + IL-6) or pathogenic (IL-6+IL-23+IL-1β) conditions with either vehicle, high salt + vehicle, or high salt + FICZ. Frequency of CCR6 expression of total CD4$^+$ T cells was analyzed to determine effect of salt and AhR activation on CCR6 regulation. ns, not significant ($p>0.05$); $*p\leq0.05$; $**p\leq0.01$; $**$

$*p \leq 0.001$; $****p \leq 0.0001$; Two-way ANOVA (A, B, F, and G) and student's two-tailed t test or Mann-Whitney U-test (C, E).

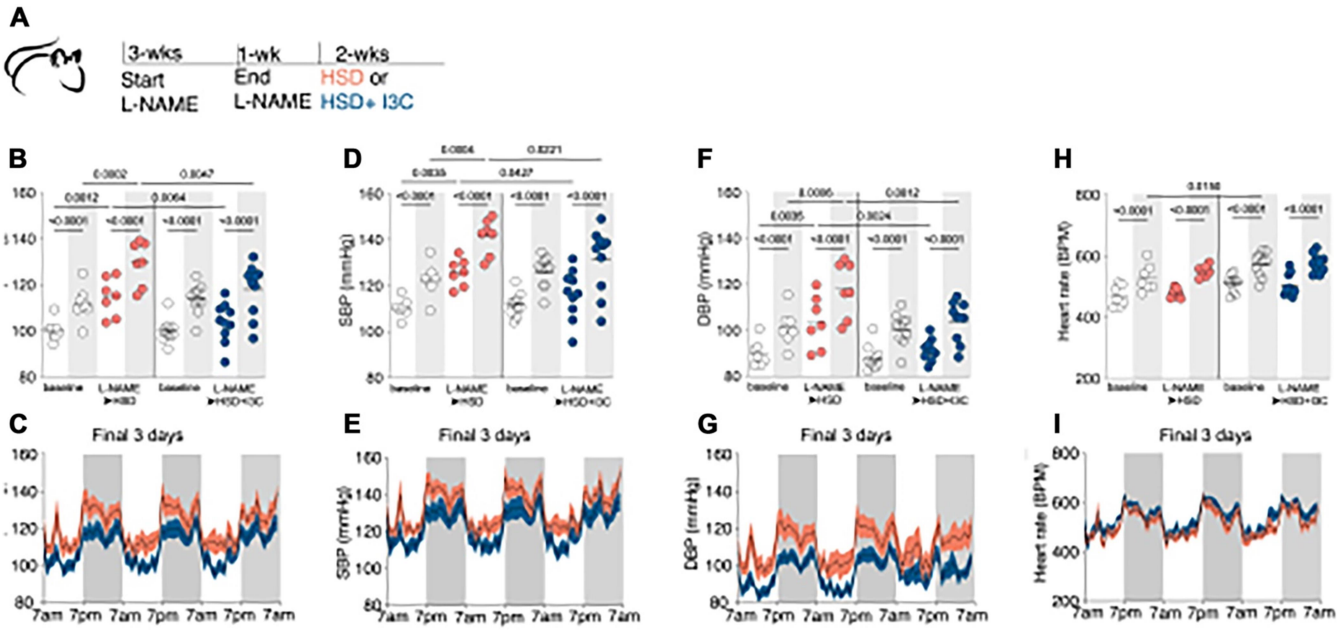

Figure 4. AhR activation restrains the development of experimental salt-sensitive hypertension. A) Experimental scheme for analysis of mice with implanted telemeters fed either a HSD or a HSD + AhR activator (I3C). Mice were implanted with telemeters, allowed to recover for at least 10-days followed by day-night analysis of mean arterial, systolic, and diastolic blood pressure recordings between baseline and paired HSD-fed mice or HSD + AhR activator (I3C)-fed mice during final 3-days of experimental protocol. B) Analysis of day (white box) and night (gray box) mean arterial pressure (MAP, mmHg) showing comparison of baseline (pre-L-NAME) with HSD-fed (orange) and HSD+AhR activator (I3C)-fed (blue) mice. C) MAP tracing averages for final 72hrs analysis of MAP final 3-day (day and night) average between HSD-fed (orange) and HSD + AhR activator (I3C)-fed (blue) mice. D) Analysis of day and night systolic blood pressure (SBP, mmHg) showing comparison of baseline (pre-L-NAME) with HSD-fed (orange) and HSD+AhR activator (I3C)-fed (blue) mice. E) SBP tracing averages for final 72hrs analysis of MAP final 3-day (day and night) average between HSD-fed (orange) and HSD + AhR activator (I3C)-fed (blue) mice. F) Analysis of day and night diastolic blood pressure (DBP, mmHg) showing comparison of baseline (pre-L-NAME) with HSD-fed (orange) and HSD+AhR activator (I3C)-fed (blue) mice. G) DBP tracing averages for final 72hrs analysis of

MAP final 3-day (day and night) average between HSD-fed (orange) and HSD + AhR activator (I3C)-fed (blue) mice. H) Analysis of day and night heart rate (HR, bpm) showing comparison of baseline (pre-L-NAME) with HSD-fed (orange) and HSD+AhR activator (I3C)-fed (blue) mice. I) HR tracing averages for final 72hrs analysis of MAP final 3-day (day and night) average between HSD-fed (orange) and HSD + AhR activator (I3C)-fed (blue) mice. Paired Two-way ANOVA (B-I).